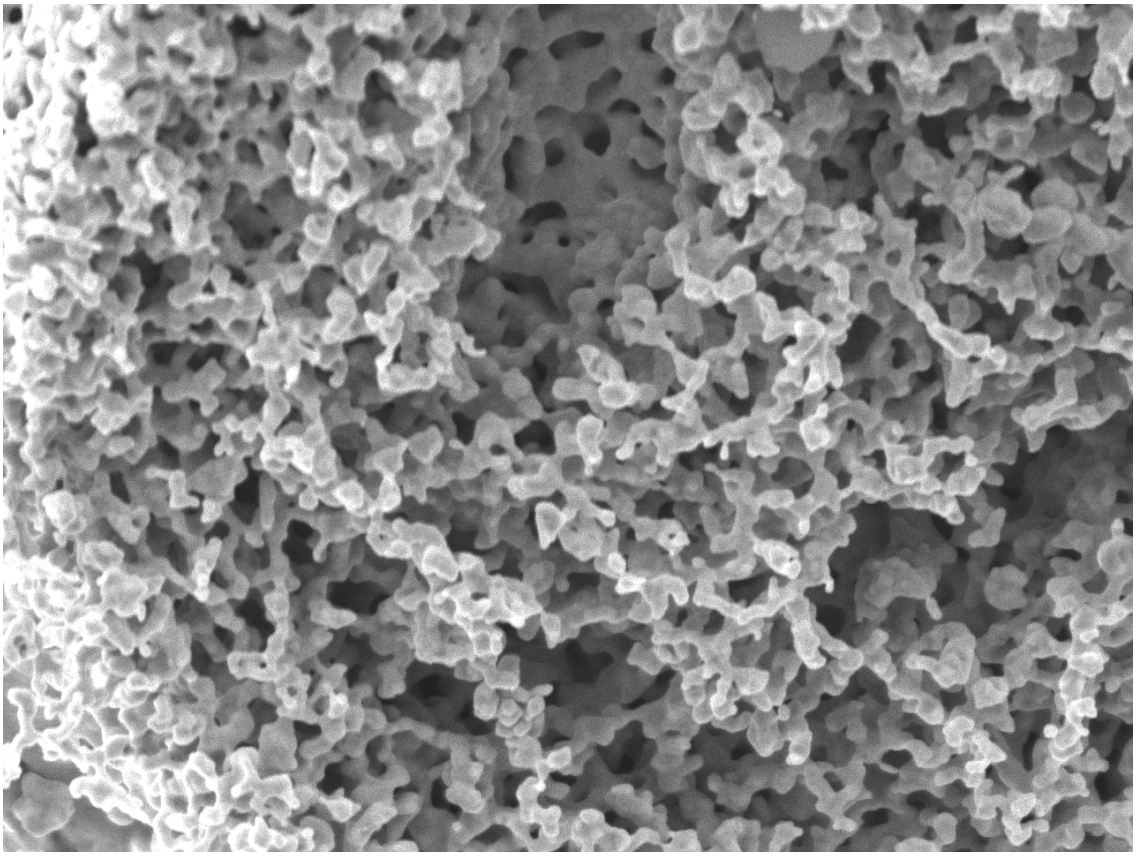

Fabrication and characterization of gold microbiosensors for enzyme-based single-site amperometry at neural spheroids

Master's thesis in Materials Chemistry

VIKTOR PREINITZ GÄRDINGE

DEPARTMENT OF CHEMISTRY AND CHEMICAL ENGINEERING

CHALMERS UNIVERSITY OF TECHNOLOGY
Gothenburg, Sweden 2026
www.chalmers.se

Master's thesis 2026

Fabrication and characterization of gold microbiosensors for enzyme-based single-site amperometry at neural spheroids

VIKTOR PREINITZ GÄRDINGE



CHALMERS
UNIVERSITY OF TECHNOLOGY

Department of Chemistry and Chemical Engineering
Division of Chemistry and Biochemistry
Chalmers University of Technology
Gothenburg, Sweden 2026

Fabrication and characterization of gold microbiosensors for enzyme-based single-site amperometry at neural spheroids
Viktor Preinitz Gärdinge

© Viktor Preinitz Gärdinge, 2026

Supervisor: Ajay Pradhan, Division of Chemistry and Biochemistry

Examiner: Ann-Sofie Cans, Division of Chemistry and Biochemistry

Master's thesis 2026
Department of Chemistry and Chemical Engineering
Division of Chemistry and Biochemistry
Chalmers University of Technology
SE-412 96 Gothenburg
Sweden
Telephone +46 (0)31-772 1000

Cover: SEM image of a nanoporous gold electrode at 16 000x magnification.

Acknowledgements, dedications, and similar personal statements in this thesis, reflect the author's own views.

Fabrication and characterization of gold microbiosensors for enzyme-based single-site amperometry at neural spheroids

Viktor Preinitz Gärdinge

Department of Chemistry and Chemical Engineering
Chalmers University of Technology

Abstract

Neurotransmitters are vital chemicals that neurons use to communicate with each other. Our understanding of how neurons send these signaling molecules to each other is essential not only for neuroscience in general, but also for our understanding of neurodegenerative diseases such as Alzheimer's. Such diseases are known to alter the transmission of several neurotransmitters, such as dopamine, acetylcholine and glutamate, among others. Characterizing the release events is therefore relevant in the research of such diseases, and this can be done with electrochemical sensors. Carbon fiber electrodes have been successfully used to detect dopamine, but since acetylcholine and glutamate do not readily undergo a redox reaction on the electrode surface, their detection requires that the sensor is fitted with enzymes that can react with these neurotransmitters to produce the reporter molecule hydrogen peroxide. Gold is more sensitive to hydrogen peroxide than carbon fiber, and, due to its high conductivity, could also provide a better signal-to-noise ratio, which is crucial for uncovering the dynamics of neurotransmitter release. In this thesis, gold microwire electrodes were fabricated and characterized for further development into amperometric biosensors that can be used to detect neurotransmitter release in biological samples. Their electrochemical function was characterized with cyclic voltammetry (CV) and amperometry, and their surfaces were characterized by SEM and EDX. A nanoporous surface layer was formed on one electrode, which resulted in an electrochemically active surface area over twice as big as that of an unmodified electrode. The nanoporous electrode was shown to be more sensitive to amperometric hydrogen peroxide detection, and gave a stronger signal in CV and square wave voltammetry. The success rate for electrodes fabricated with a micropipette puller was 61%. Aside from these disc shaped electrodes, the pipette puller was also used to produce gold nanotip electrodes in a single step without the need for further tip shaping of any kind, which, to the best of the author's knowledge, has not been described before. Further work is needed to optimize the nanopore formation protocol as well as to increase the success rate of electrode fabrication by the micropipette puller method. The behavior of these electrodes when fitted with the appropriate enzymes is yet to be characterized.

Keywords: Biosensor, gold, nanoporous gold, electrode, neurotransmitter, acetylcholine, amperometry

Acknowledgements

I would first like to thank my supervisor, Ajay Pradhan, whose guidance has been endlessly helpful in completing this work. I would also like to thank my examiner, Ann-Sofie Cans, for offering me the opportunity to work on this project. Further, I want to thank the people at CMAL for allowing me to use one of their SEM machines, which was crucial for the project. Finally, I want to thank everyone on the 9th floor in research building 1, where most of the work was carried out. They all contributed to a welcoming and friendly work environment.

Viktor Preinitz Gärdinge, Gothenburg, June 2026

Contents

List of abbreviations **v**

List of figures **vi**

List of tables **viii**

1 Introduction **1**
1.1 The brain and neurotransmitters . . . 1
1.2 Sensitive monitoring of neurotransmitters with electrochemistry . . . 2
1.3 Aim and limitations . . . 3

2 Background **4**
2.1 Methodology . . . 4
2.1.1 The electrochemical cell . . . 4
2.1.2 Electrode fabrication . . . 4
2.1.3 Amperometry . . . 4
2.1.4 Cyclilc voltammetry . . . 4
2.1.5 Measuring surface area electrochemically . . . 5
2.1.6 Formation of nanoporous gold (NPG) . . . 5
2.1.7 Scanning electron microscopy . . . 6
2.1.8 Energy dispersive X-ray spectroscopy (EDX) . . . 6
2.1.9 Square wave voltammetry (SWV) . . . 7

3 Experimental section **8**
3.1 Electrode fabrication . . . 8
3.1.1 Plastic electrodes . . . 8
3.1.2 Glass electrodes . . . 9
3.1.3 Pulled glass encased electrodes . . . 10
3.2 Electrochemical methods . . . 13
3.2.1 Cyclic voltammetry . . . 13
3.2.2 Amperometry . . . 14
3.2.3 Surface cleaning . . . 14
3.2.4 Surface area measurement . . . 14
3.2.5 NPG formation by alloying/dealloying . . . 14
3.2.6 NPG formation by anodization . . . 15
3.3 Surface characterization by SEM . . . 15

4 Results and discussion **16**
4.1 Plastic electrodes . . . 16
4.2 Glass electrodes . . . 18
4.2.1 The effect of potential range and salt bridge on the unknown peaks . . . 19
4.2.2 Surface area measurements . . . 21
4.2.3 Insulation method #1: epoxy + paraffin wax . . . 22
4.2.4 Insulation method #2: phenol, 2-allylphenol copolymer + epoxy . . . 23

4.2.5 Insulation method #3: Nafion™ + epoxy 24
4.2.6 NPG formation by dealloying 24
4.2.7 NPG formation by anodization 25
4.3 Pulled glass encased electrodes (P-1000) 26
4.3.1 Nanotip electrodes 26
4.4 Pulled glass encased electrodes (P-2000) 27
4.5 Pulled glass encased (P-2000) NPG electrodes 29
4.5.1 Amperometry 31
4.5.2 Electrolyte effects 33
4.5.3 Surface area measurements 35

5 Conclusion and future work **37**
5.1 Conclusions 37
5.2 Future work 37

6 Appendix **41**
6.1 Voltammograms for real surface area determination 41
6.2 EDX images of failed NPG electrodes 41
6.3 SEM images of the NPG electrode for determination of A_{geo} 42

List of abbreviations

Below is an alphabetically ordered list of abbreviations used in this thesis.

CE	Counter electrode
CV	Cyclic voltammetry
EDX	Energy dispersive X-ray spectroscopy
NPG	Nanoporous gold
PBS	Phosphate buffered saline
PET	Positron emission tomography
RE	Reference electrode
SE	Secondary electron
SEM	Scanning electron microscopy
SWV	Square wave voltammetry
WE	Working electrode

List of Figures

1 Schematic diagram of neurotransmitter exocytosis, showing both kiss-and-run and full fusion. Adapted from [1]. 1
2 Visualization of nanopore formation in gold by alloying and dealloying with zinc. . . 6
3 Diagram showing the potential profile in SWV. 7
4 Illustration showing how electrodes are fabricated with a micropipette puller. 8
5 Illustration of the steps to assemble the glass electrodes. 10
6 A representative example of a usable pulled electrode under a microscope and where to cut them. 11
7 Illustration of the electrode beveling process. 12
8 Photographs of the three types of electrode, with black and red markings to differentiate them from other electrodes of the same type. (a) Plastic, (b) glass, (c) pulled glass encased. 13
9 CV in 1 mM FcMeOH and 100 mM KCl before and after cleaning one of the three plastic electrodes. 16
10 CV in 10 mM PBS before and after cutting one of the three plastic electrodes a number of times. 17
11 CV in 1 mM FcMeOH and 100 mM KCl before and after cutting one of the plastic electrodes. 18
12 CV in 1 mM FcMeOH and 100 mM KCl for some of the glass electrodes. 19
13 Illustration of the setup for the salt bridge tests. 20
14 A representative CV recorded with the salt bridge setup. 20
15 Repeated CVs in 1 mM ferrocenemethanol, 100 mM KCl *vs* Ag|AgCl for a glass electrode, each cycle having a higher initial potential than the last. Inset: a zoomed-in view of the unknown anodic peak. 21
16 CV in 1 mM FcMeOH and 100 mM KCl for a glass electrode after epoxy and paraffin coatings. 22
17 CV in 1 mM FcMeOH and 100 mM KCl for a glass electrode after phenol-allylphenol copolymer and epoxy coatings. 23
18 CV in 1 mM FcMeOH and 100 mM KCl for a glass electrode before and after Nafion™ and epoxy coatings. 24
19 SEM images of one of the failed dealloyed NPG electrodes. 25
20 SEM images of one of the failed anodized NPG electrodes. 25
21 SEM images of the three nanotip electrodes. Scale bar = 1 µm. 26
22 CV responses of the three gold nanotip electrodes in 1 mM FcMeOH and 100 mM KCl. 27
23 Representative CV of a laser pulled electrode in 1 mM ferrocenemethanol and 100 mM KCl. 28
24 SEM images of a pulled glass encased electrode. Scale bar = 10 µm (a), and 1 µm (b). 29
25 SEM images of a failed NPG electrode. Scale bars = 1 µm. 30
26 SEM images of the successful NPG electrode. Scale bars = 10 µm (a), and 1 µm (b). 30
27 SEM images of two unsuccessful NPG electrodes. Scale bars = 10 µm 31
28 i-t curves of non-NPG (a) and NPG (b) electrodes at different potentials in 10 mM PBS and 10 mM H_2O_2 at an applied potential of 0.5 V. 32

29 i-t curves of non-NPG (a) and NPG (b) electrodes at different potentials in 10 mM PBS and 10 mM H_2O_2 at an applied potential of 0.8 V. 32
30 CV in 1 mM ferrocenemethanol and 100 mM KCl, *vs* Ag|AgCl of the NPG electrode prior to and after NPG formation. 33
31 CV recorded in 5 mM $K_3Fe(CN)_6$ and 0.1 M KCl, with the NPG electrode and an unmodified electrode for reference. 34
32 SWV of the non-NPG and NPG electrodes. 35
33 CVs recorded in 0.5 M H_2SO_4 at 0.1 V/s 41
34 EDX images of the failed NPG electrode in figure 27a. Scale bars = 10 µm 41
35 EDX images of the failed NPG electrode in figure 27b. Scale bars = 10 µm 42
36 SEM image of the successful NPG electrode from a different angle. Scale bar = 1 µm. 42

List of Tables

1 Geometric areas of six pulled glass encased electrodes, based on SEM images. 29
2 Amperometric responses of NPG and non-NPG electrodes at different potentials in 10 mM PBS and 10 mM H_2O_2 33
3 Current amplitudes for the non-NPG and NPG electrodes in the CV shown in figure 31, at -0.2 V 34

1 Introduction

1.1 The brain and neurotransmitters

Much of the brain is composed of neurons, which number in the tens of billions. Collective neuronal activity gives rise to complex biological phenomena such as cognition, memory, awareness, and behavior, among others. To carry out these functions, neurons communicate with each other by sending signaling chemicals, called neurotransmitters, to each other. For this purpose, neurons have extensions from the main cell body which can release and receive neurotransmitters. The releasing extension is called the axon, and the receiving extensions are called dendrites. The axons and dendrites meet at the neuronal synapses, which contain a 20 nm gap called the synaptic cleft, across which neurotransmitters are relayed. The neurotransmitters are first packaged in 40 nm synaptic vesicles inside the neurons, which are brought to the end of the axon of the presynaptic neuron, where they fuse with the cell membrane to form a fusion pore through which the neurotransmitters are expelled into the synaptic cleft. They then diffuse across the cleft and bind to receptors on the dendrites of the postsynaptic neuron, which triggers a response in this cell, thus, chemically transmitting signals between neurons.

Neurotransmitter release occurs *via* exocytosis, a general term for when vesicles loaded with cellular material and signaling molecules fuse with the cell membrane to release its contents outside the cell. Neurotransmitter exocytosis is a dynamic phenomenon and several different release profiles can be observed. For example, in full fusion the vesicle fuses completely with the membrane, causing the entire neurotransmitter load to be released. In contrast to this, there is also kiss-and-run fusion, where the fusion pore closes and the vesicle detaches from the cell membrane after only part of its content has been released. These release profiles are shown schematically in figure 1.

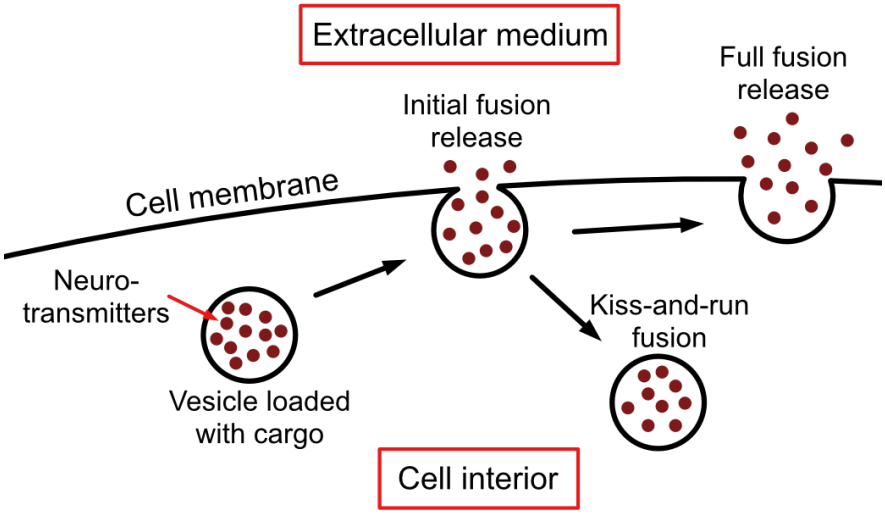

Figure 1: Schematic diagram of neurotransmitter exocytosis, showing both kiss-and-run and full fusion. Adapted from [1].

As neurotransmitter release dynamics serves as the basis for neuronal communication, through fine-tuned control over signaling strength, it is important for understanding how the human brain works. Further, altered neurotransmission is associated with a variety of diseases including neurodegenerative diseases like Alzheimer's.

Different strategies have been employed to study neurotransmission, including PET imaging, fluorescence microscopy, mass spectrometry-based methods, microdialysis, and electrochemical methods such as amperometry and voltammetry [2]. Advantages such as high temporal resolution, low implementation cost, and relatively high sensitivity, make electrochemical methods highly attractive for studying neurotransmitter dynamics, and are thus chosen for this project. The release of neurotransmitters *via* exocytosis can be studied using amperometric electrodes *via* the redox reactions of neurotransmitters such as dopamine at the electrode surface. The technique has been successfully applied in the study of electroactive neurotransmitters like dopamine and serotonin, but other important neurotransmitters like acetylcholine and glutamate, important for memory and learning, do not readily undergo such a reaction at the electrode surface on their own. Therefore, their detection requires the generation of the electroactive reporter molecule hydrogen peroxide. This is achieved by anchoring enzymes at the electrode surface, which produce hydrogen peroxide from the analyte.

1.2 Sensitive monitoring of neurotransmitters with electrochemistry

Electrochemical sensors can continuously record the resulting current generated in a redox reaction when a constant potential is applied to it. This method is called amperometry which is able to detect exocytotic neurotransmitter release in real time. Differences in the measured signals can be seen depending on which release profile describes the event, provided that the sensor is sensitive enough. The initial vesicle-membrane fusion appears as a small "foot" at the base of the main current spike, which is the result of the neurotransmitters leaking immediately upon pore formation. However, this fusion signal is easily lost in the background noise due to its small amplitude, making sensitivity an important design requirement in the fabrication of neurotransmitter sensors.

There are several factors that affect the sensitivity of a sensor. One such factor is the material the sensor is made of. Carbon fiber has been a staple material for constructing neurotransmitter sensors due to its low cost, biocompatibility, good electrochemical properties, and the ease and reproducibility of the fabrication of such electrodes [3], [4]. They have been successfully used for the detection of dopamine, but for hydrogen peroxide detection, which, as previously stated, is necessary for the detection of acetylcholine and glutamate, metals like gold and platinum are significantly more sensitive. This has led to the development of carbon fiber electrodes surface-modified with metal nanoparticles [4], but pure noble metal electrodes could in theory provide a better signal-to-noise ratio due to their high conductivity in conjunction with their native ability to detect hydrogen peroxide. The increased signal-to-noise ratio of such an electrode could solve the problem of resolving the low amplitude foot feature prior to the event spike caused by the rapid initial leakage of neurotransmitters. Additionally, modification of the metal surface with metal nanoparticles or the creation of nanopores can dramatically increase the surface area and catalytic efficiency, which would further improve the sensitivity of the sensor. The porosity of nanoporous gold also makes it

good at trapping biomolecules like enzymes [5], making them good candidates for enzymatic sensors, which are needed for the detection of acetylcholine and glutamate, as previously mentioned. Further, nanoporous gold microbiosensors have so far had limited application in acetylcholine detection, and may have untapped potential for this purpose.

1.3 Aim and limitations

The main aim of this project was to establish an efficient and reproducible protocol for the fabrication of gold microbiosensors, which were ultimately to be used for acetylcholine detection *in vitro*. Because of this, their ability to amperometrically and sensitively detect hydrogen peroxide was an ultimate design requirement. High sensitivity to hydrogen peroxide is, as previously mentioned, a native property of gold when compared with carbon fiber, but the sensitivity was also to be increased further by the formation of a nanoporous layer on the gold electrode, drastically increasing its electroactive surface area.

The main limitation of the project comes from the lack of time to fully develop the electrodes for their intended purpose. It was initially intended that enzymatic detection of acetylcholine was to be conducted in the final stage of the project, but this did not come to fruition, as the preceding steps took more time than anticipated. The other main limitation of the project comes from the inherent properties of gold microwires at the micrometer dimensions. At such dimensions, the conventional fabrication method of creating glass-insulated electrodes with a micropipette puller suffers from low success rate due to the extreme brittleness of the gold microwire. This leads to the fracturing of the wires during the glass-encasing step, which leads to a large waste of the expensive gold material. Although this is mitigated using innovative sensor design aimed at reducing the amount of gold used per electrode, it is nonetheless non-ideal. Additionally, potential chloride contamination of the gold working electrode from the reference electrode and electrolyte are additional limitations which are difficult to address currently.

2 Background

2.1 Methodology

2.1.1 The electrochemical cell

The electrochemical techniques described herein, such as amperometry and cyclic voltammetry, all take place in electrochemical cells. The cell consists of a small volume of an ionically conductive solution called the electrolyte. The ions in the electrolyte carry electric current between electronic conductors called electrodes, which are connected to a potentiostat. The potentiostat controls the potential of the working electrode (WE), measured with reference to the reference electrode (RE), and the electrical circuit is completed through the counter electrode (CE). If the electrical resistance of the solution is negligible, and if the current regenerated is small, the RE can take the role of CE as well. In this project, the fabricated gold electrodes take the role of WE.

2.1.2 Electrode fabrication

At the most basic level, the electrodes described in this work are fabricated by connecting a gold microwire to a silver wire and insulating the assembly such that only a small part of the gold surface is exposed and available for electrochemical interactions, while the silver wire is completely insulated. The purpose of the silver wire is to allow for a sturdy connection to the potentiostat which the brittle gold wire could not offer, as well as to reduce the amount of gold used. Three types of electrodes were fabricated: plastic insulated electrodes, glass and epoxy insulated electrodes, and glass encased electrodes without epoxy insulation, fabricated with a micropipette puller. For the sake of brevity, these three types of electrodes will be referred to as plastic electrodes, glass electrodes, and pulled glass encased electrodes, respectively. The order in which the gold wire is insulated and connected to the silver wire necessarily differs between the methods, and detailed descriptions of their fabrication is left to the Experimental section 3.

2.1.3 Amperometry

In amperometry, the applied potential on the WE is fixed, while the current is measured over time. When an analyte comes into contact with the WE it undergoes a redox reaction, i.e. a charge transfer, causing an increase in the amplitude of the measured current. Thus, the amount of charge transferred, and therefore the concentration of analyte, can be related to the current signal. Amperometry has high sensitivity and temporal resolution, making amperometric biosensors highly attractive for studying exocytosis.

2.1.4 Cyclilc voltammetry

Cyclic voltammetry (CV) is a technique that can be used to study electron transfer processes, such as redox reactions of chemical species. The applied potential to the WE is varied, being swept from a lower limit to a higher limit (or from high to low), and then back, for one or more cycles. This results in a changing current that is measured. Plots of these data can then be analyzed, where peaks in the measured current are associated with electrochemical changes. CV measurements can

show that the gold electrodes fabricated in this project are able to carry out redox reactions on their surfaces reliably.

2.1.5 Measuring surface area electrochemically

There are two important surface areas to consider: the geometric area and the real area. The geometric area is the simplest to measure as it is a macroscopic approximation that does not take microscopic topography into account. For example, though paper is known to be porous and have a microscopically rough surface of interwoven cellulose fibers, a sheet of A0 paper is considered to have a geometric surface area of 1 m^2 (per side), as if it were perfectly flat, since this is the result of multiplying the lengths of its edges. However, the real surface area is larger than this, due to the aforementioned porous nature of the material. In the case of paper, this difference may be negligible and irrelevant, but for microelectrodes the surface area of the electrode is an important parameter that influences its performance, particularly its sensitivity. Larger electrodes give rise to larger currents which are less likely to be lost in background noise, but if they are to be placed in synaptic clefts their size is strongly restricted. To make the electrodes more sensitive then, a viable method is to increase its surface area by giving it a rougher topography on the nanoscale, for example by forming nanosized pores. How this is done is described below in section 2.1.6. The rest of this section describes how the real surface area can be measured electrochemically.

There are a few electrochemical methods for determining the surface area of an electrode, such as relating it to the surface's double layer capacitance or measuring the amount of adsorbed probe molecules [6]. In this project, one of the simplest techniques is used, the oxide layer formation method. This makes use of the natural oxidation and reduction of the gold surface during potential cycling. As the potential is raised, an oxide monolayer forms, and when the potential is lowered, the oxide layer is reduced. The current peak associated with the reduction of the oxide layer is integrated to acquire the charge associated with it, and this is compared with the known charge density associated with the reduction of a monolayer of gold oxide to deduce the real surface area. In an article examining different methods of determining the real surface area of nanoporous gold and palladium electrodes, Do, Seland and Johannessen found that the oxide formation and double layer capacitance methods gave the largest measurements, and these values were similar, meaning the methods corroborate each other [6]. The surface oxide method is a popular choice for measuring the surface area of nanoporous gold electrodes [7], [8], [9].

2.1.6 Formation of nanoporous gold (NPG)

Nanoporous gold (NPG) is a type of material with promising properties and applications in sensing and catalysis [10]. It is characterized by a network of gold ligaments and voids, with pore diameters typically ranging from 10 to a few 100 nm [10], [11]. The high surface curvature and low coordination number of surface atoms give NPG its catalytic activity, while its advantages in sensing come from the higher electrochemically active surface area and a lower impedance compared to morphologically homogeneous electrodes, which results in a better signal-to-noise ratio [12]. Several methods for producing NPG have been devised, such as templating and solution mediated synthesis [10], but the most common method is dealloying with a less noble metal [13], which was the chosen method for this project. The homogeneous gold electrode is immersed in an electrolyte containing the sacrificial

metal, in this project zinc, and the electrode potential is first swept to low values to form an alloy surface layer. When the potential is swept to higher values the zinc is dissolved once more, leaving voids behind in the gold structure. This cycle is repeated a number of times to successively carve out the bicontinuous, nanoporous structure in the electrode surface. This process is visualized in figure 2. Another, related method that was also attempted in this project was the anodization method. The principle is similar to the dealloying method, but instead of alloying the surface with another metal, the surface is oxidized with a positive potential sweep, and the oxide layer is then reduced with a negative sweep, leaving a porous structure behind.

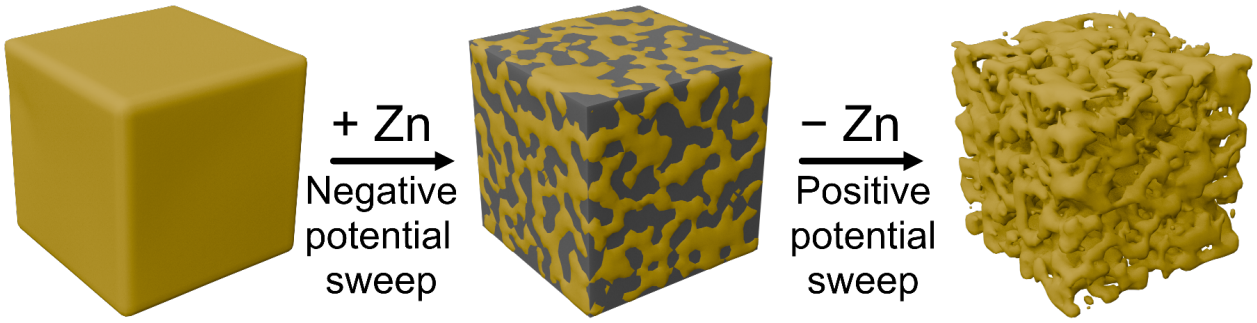

Figure 2: Visualization of nanopore formation in gold by alloying and dealloying with zinc.

To determine whether the procedure for producing the NPG layer was successful, scanning electron microscopy was used to get a clear image of the electrode surface. To quantify the roughness and find out how much the real surface area was increased, the roughness factor was also obtained. This quantity is defined as the real area divided by the geometric area.

2.1.7 Scanning electron microscopy

In scanning electron microscopy (SEM), electrons are released from a heated filament, accelerated by an applied potential, and focused by electromagnetic lenses to form a precise electron beam, which is raster scanned across a sample. The electrons interact with the atoms in the sample in different ways to generate different types of signals, and the intensity of these signals is represented by the brightness of the resulting pixels, forming an image. For the investigation of surface morphology, secondary electrons (SE) are the signal type used. SEs are electrons that are "knocked out" of the sample when the beam of primary electrons collides with it. The SEs have a relatively short mean free path, meaning they cannot travel very far within the sample material before recombining. Because of this, the detected SEs only come from the top few nanometers of the sample, and are therefore good for imaging the topography of the sample.

2.1.8 Energy dispersive X-ray spectroscopy (EDX)

The elemental composition of a sample can be estimated with energy dispersive X-ray spectroscopy (EDX). A high energy beam of either electrons or X-rays is scanned over a sample in a similar manner as in SEM, and this incident beam excites inner shell electrons to the point of ionization, leaving a low energy orbital empty. This orbital is filled by an electron from a higher energy

level, and this transition results in the emission of an X-ray with an energy equal to the difference between the two energy levels. Since elements have unique atomic structures, the X-rays emitted from different elements have characteristic energies, allowing for elemental determination.

2.1.9 Square wave voltammetry (SWV)

In square wave voltammetry (SWV) the current is measured as the potential applied to the WE is pulsed while also steadily increasing. The potential profile is a superposition of a staircase-shaped sweep and a square wave, hence the name of the technique. The potential profile is shown in figure 3. The current is measured twice per cycle, once at the peak and once in the valley of the square wave, and the difference between these currents is plotted as a function of the potential. A benefit of this technique is that it is very effective at screening off background currents, more so than CV.

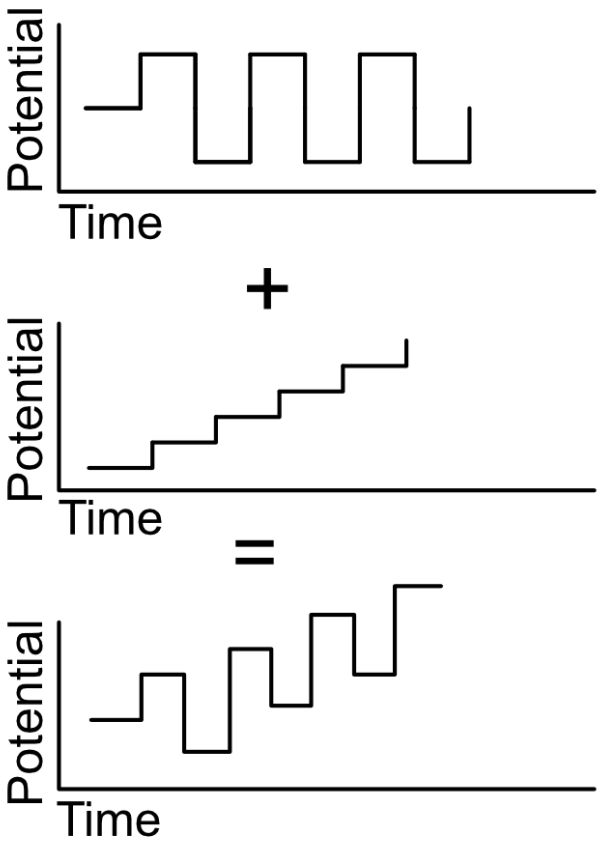

Figure 3: Diagram showing the potential profile in SWV.

3 Experimental section

3.1 Electrode fabrication

The main method for producing carbon fiber electrodes of the type used in this work is by inserting the fiber in a glass capillary and pulling it apart with a micropipette puller, yielding two glass-insulated electrodes. The puller heats up the middle section of the capillary to melt it before pulling the ends apart, causing the glass to taper and tightly seal the wire inside. This is showed schematically in figure 4. However, gold microwire is far less tough than carbon fiber and is thus much more prone to breaking during the pulling step, and the settings on the machine must be optimized to minimize the waste of precious metal wire. The use of this method was therefore reserved for later in the project, following experience with gentler approaches.

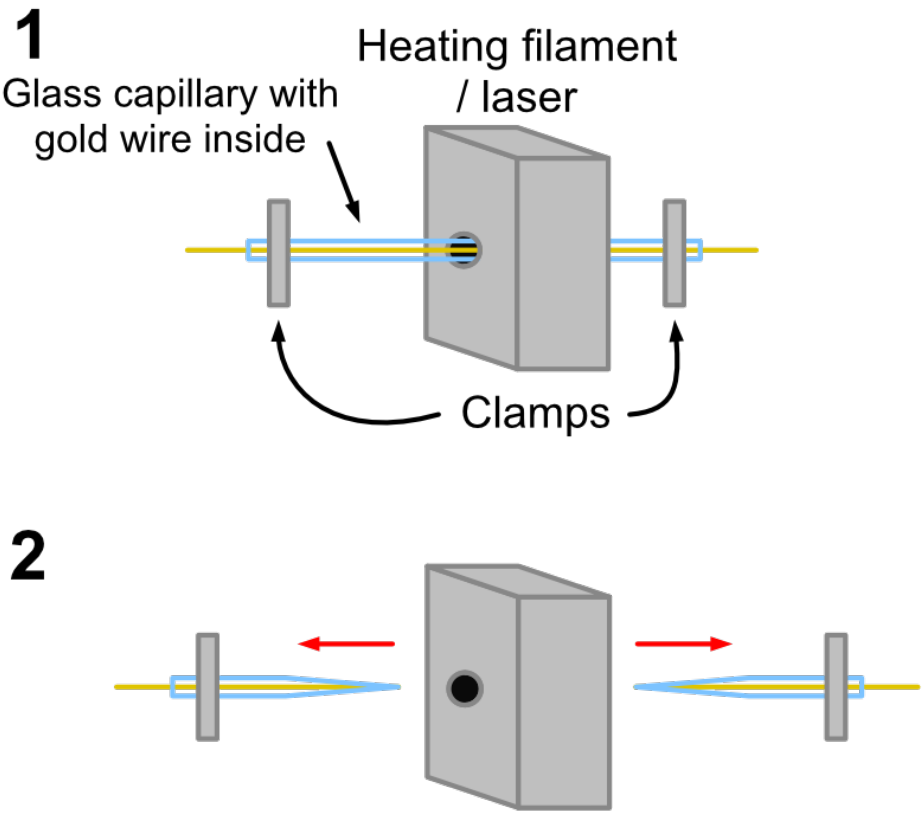

Figure 4: Illustration showing how electrodes are fabricated with a micropipette puller.

3.1.1 Plastic electrodes

Roughly 1 cm of gold wire ($\geq$ 99.99%, 25 µm diameter, Sigma-Aldrich, USA) was cut and glued to silver wire ($\geq$ 99.99%, 250 µm diameter, Sigma-Aldrich, USA) using a colloidal silver paste, by dipping the silver wire in the paste and then joining the wires together. The wires were left overnight at room temperature to let the paste dry. Then, the wires were each inserted, silver end of the wire

first, into the larger end of 100 µl plastic pipette tips that had been cut to size. Epo-Tek® 301 epoxy resin and hardener (Epoxy Technology Inc., USA) were mixed at a 4:1 ratio and inserted in the tips before the wire was pulled backwards through the tips until about 2 mm of gold wire was immersed in the epoxy, ensuring that the silver part of the wire was completely insulated.

3.1.2 Glass electrodes

Gold and silver wires were cut and glued as described above. Borosilicate glass capillaries (Harvard Apparatus Ltd., UK) with dimensions 10 cm length, 1.5 mm OD and 1.17 mm ID were cut to a length of roughly 3 cm and the wires were partially inserted such that the entire gold wire and part of the silver wire were outside the capillary. Epoxy resin was inserted by dipping the capillary and letting the resin rise *via* capillary action. Prior to this, the exposed silver wire was bent to ensure the gold wire did not come into contact with the mixture. When the capillary was sufficiently filled, the wire was straightened again and inserted until roughly 2 mm of the gold wire was immersed. The electrodes were placed in a leaning holder or taped vertically to the side of one in order to keep the epoxy in the correct end of the capillary under gravity. The holder was then placed in an oven at 100°C overnight to cure the epoxy. The assembly of the electrodes is shown schematically in figure 5.

Electrodes fabricated with this method have relatively large and variable surface areas, which ideally need to be minimized in a controlled way. To do this, the gold wire may be completely insulated and then cut to reveal a circular interface with the same diameter as the wire without having any exposed gold on the sides of the wire. Three different insulation coatings were tested: epoxy followed by paraffin wax, 2-allylphenol and phenol copolymer base coating followed by epoxy, and Nafion™ base coating followed by epoxy.

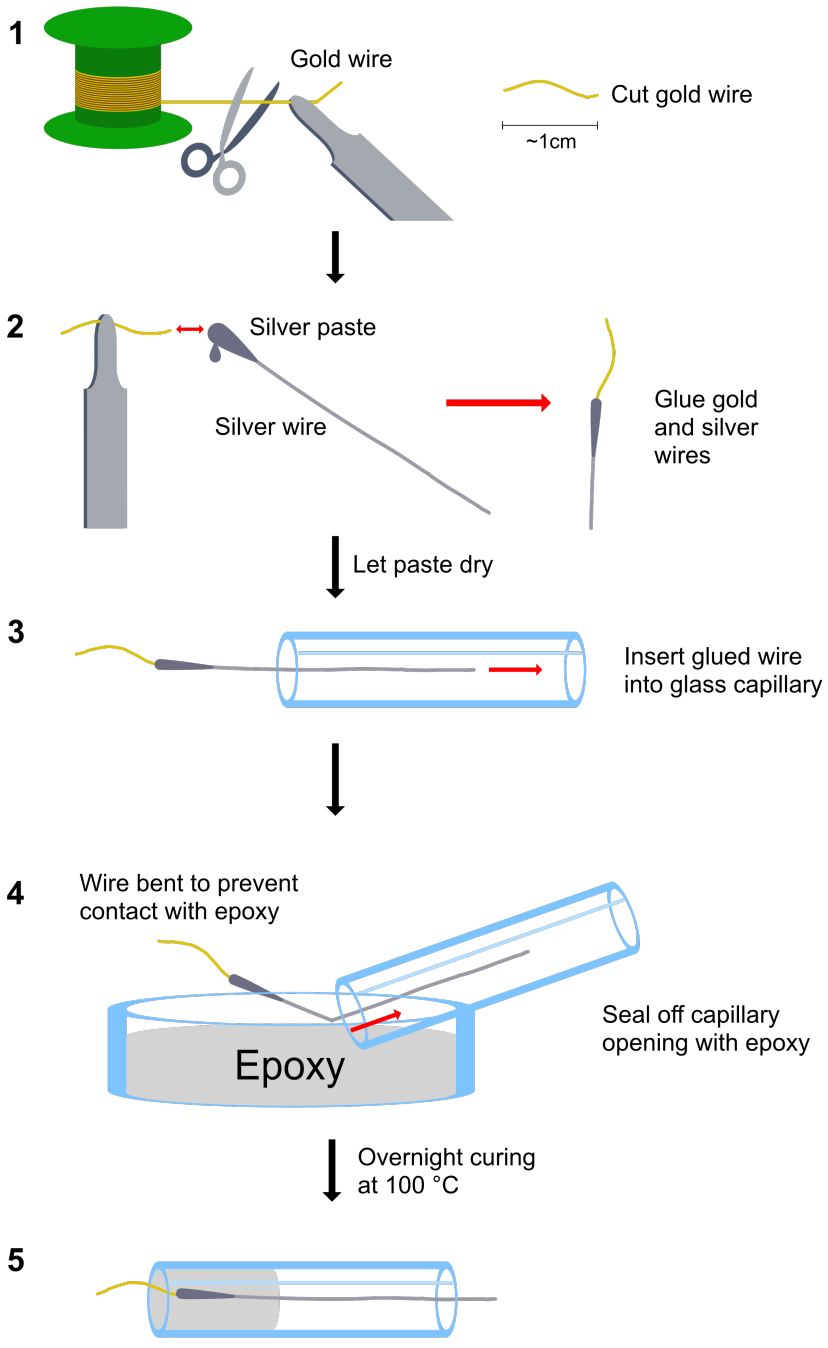

Figure 5: Illustration of the steps to assemble the glass electrodes.

3.1.3 Pulled glass encased electrodes

Borosilicate glass capillaries (Harvard Apparatus Ltd., UK) with dimensions 10 cm length, 1.2 mm OD and 0.69 mm ID were cut to a length of about 6.66 cm. Roughly 9.66-10 cm of gold wires were

cut and inserted into the capillaries using a vacuum pump. The wire was then adjusted to ensure at least 1 cm of wire protruded out of the glass at both ends. Each glass capillary with gold wire were then pulled into two glass encased electrodes using a micropette puller. Two different types of micropipette pullers were used in the project, the Model P-1000 Flaming/Brown puller (Sutter Instrument Co., USA) and the Model P-2000 laser puller (Sutter Instrument Co., USA). The P-1000 model was used initially, but due to a hardware malfunction that couldn't be quickly resolved, it was necessary to switch to the P-2000 model. After the electrodes were pulled, they were inspected with a microscope to check for breaks in the gold wire. Virtually all electrodes showed multiple breaks of the gold wire near the tip, but only breaks occurring further back where the glass diameter was large enough to no longer tightly seal the wire were considered problematic. After the unusable electrodes were discarded, the intact ones were cut at the tips to remove the portions containing breaks using a razor blade and microscope. Cuts were made at the break furthest away from the tip, as shown in figure 6.

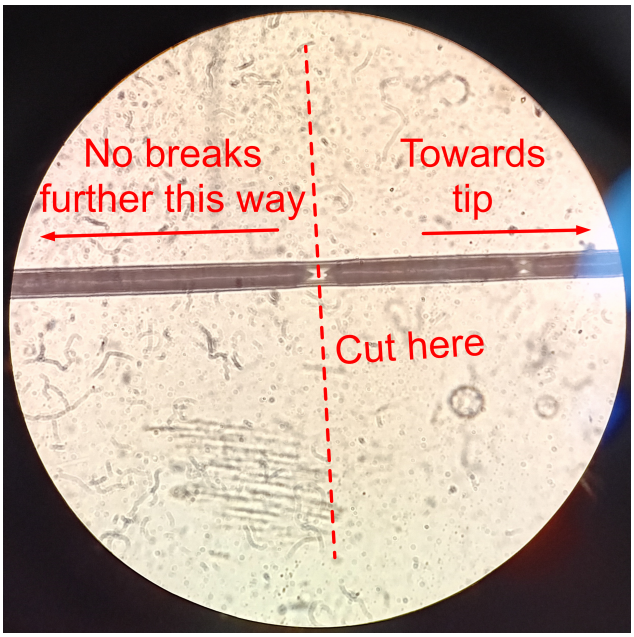

Figure 6: A representative example of a usable pulled electrode under a microscope and where to cut them.

Following the cutting step, silver wires were glued to the electrodes by dipping the silver wire in silver paste, and then partially inserting the wire in the open end of the capillary. This was done at least five times to ensure the capillary was sufficiently filled. Then, the silver wire was pushed in as far as it would go before the assembly was left to dry overnight at room temperature. The electrodes then needed to be beveled so that the exposed gold surface would be flat and uniform. To mitigate the possibility of the glass shattering during beveling, the electrode tips were first immersed in epoxy resin for 3 min, and then dipped repeatedly in acetone for 15 s to remove excess epoxy and allowed to cure at 100°C overnight in an oven. Electrodes were then beveled using a BV-10 microelectrode beveler (Sutter Instrument Co., USA) with a 104D diamond abrasive plate at a 45°

angle. To mitigate the possibility of diamond particles adhering to the gold surface, the electrode was moved up and down repeatedly rather than being pressed against the plate continuously. The beveling process is illustrated in figure 7.

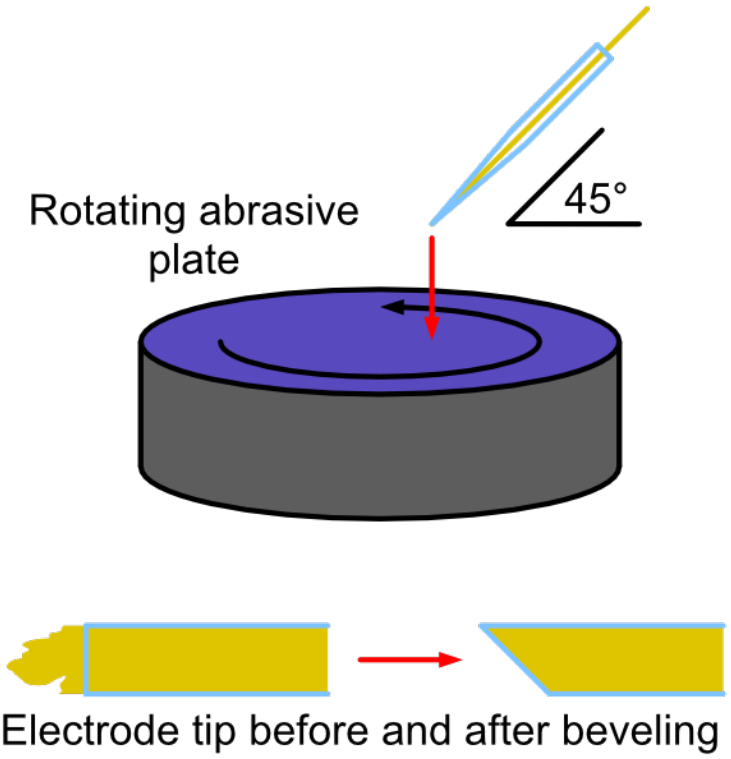

Figure 7: Illustration of the electrode beveling process.

Photographs of the three types of electrode can be seen in figure 8. The tips are all oriented toward the top of the image. The plastic (a) and glass (b) type electrodes have gold wire freely protruding at the tip, but due to its small diameter it cannot be clearly seen in the photographs.

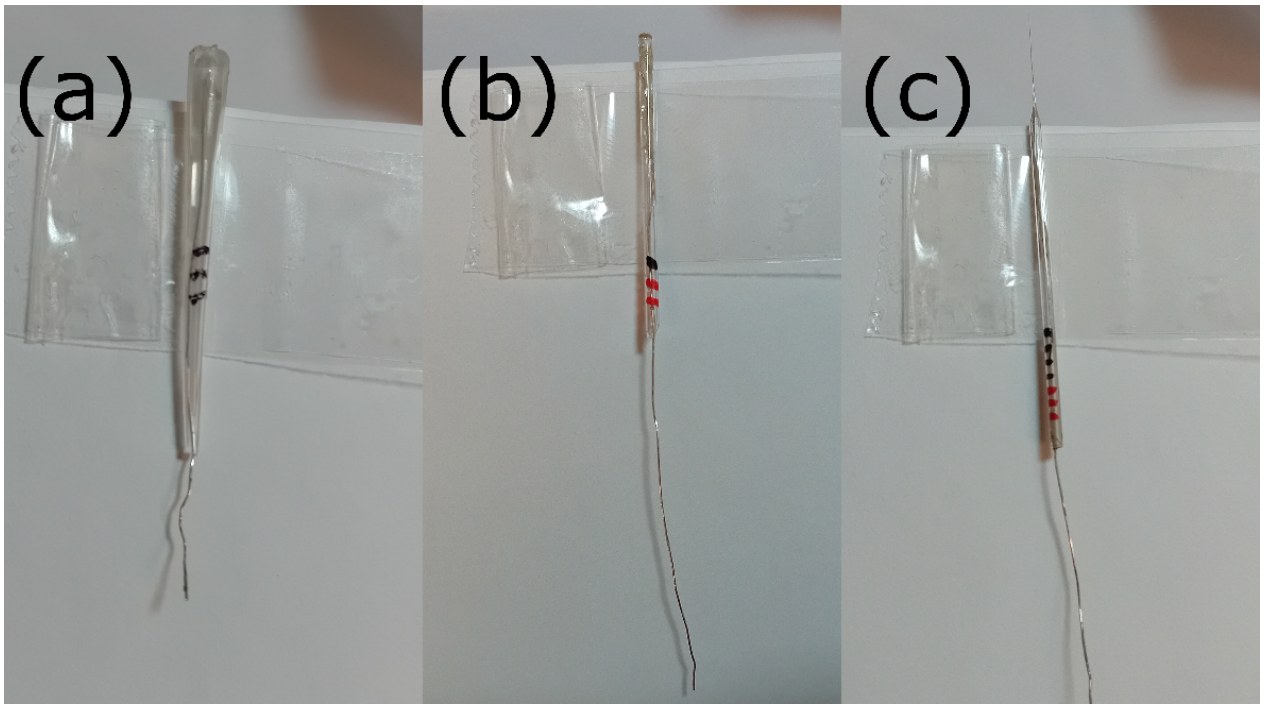

Figure 8: Photographs of the three types of electrode, with black and red markings to differentiate them from other electrodes of the same type. (a) Plastic, (b) glass, (c) pulled glass encased.

3.2 Electrochemical methods

Electrochemical methods were employed for several purposes: to test the electrodes' function, clean their active surfaces, measure the areas of their active surfaces, and generate nanopores in the exposed metal surface. All electrochemical procedures were carried out using a CHI1030C electrochemical analyzer (CH Instruments, USA), and, unless otherwise stated, a Faraday cage.

3.2.1 Cyclic voltammetry

Cyclic voltammograms were routinely recorded after electrode fabrication to test their function as well as before and after other uses, like before and after an amperometric experiment, to check if the experiment altered the electrodes' properties. These CVs were recorded in an electrolyte consisting of 1 mM ferrocenemethanol and 100 mM KCl, using an Ag|AgCl electrode (CHIII Reference Electrode, CH Instruments, USA) as a reference and a platinum wire (250 µm diameter, Sigma-Aldrich, USA) as a counter electrode. The scan rate was 0.1 V/s, the lower potential limit was -0.2 V, the upper potential limit was 0.6 V, and the potential was scanned from the lower limit to the upper, then back to the lower to complete one cycle.

3.2.2 Amperometry

Amperometric measurements were made with Pt wire as CE and Ag|AgCl as RE in 10 mM phosphate buffered saline (PBS) with a stir bar. The stirrer speed was set to 300 rpm, and the potential was held at 0.5 V and 0.8 V in separate experiments. The electrodes spent at least 10 min in peroxide-free PBS as a background measurement, after which H_2O_2 was injected to yield a 10 mM solution, and the signal was again allowed to stabilize over at least 10 min.

3.2.3 Surface cleaning

The protocol for cleaning the surface of the gold electrodes was adapted from the works of Heiskanen et al. and Fischer et al. [14], [15]. First, the electrode tips were rinsed with deionized water and immersed in a solution of 25 vol% H_2O_2 and 50 mM KOH for 10 minutes. Then, after another rinse in deionized water, a linear voltammetric sweep was carried out in a solution of 50 mM KOH with Pt wire as CE and Ag|AgCl as RE, using a scan rate of 0.05 V/s, from -0.2 V to -1.2 V.

3.2.4 Surface area measurement

A 0.5 M solution of H_2SO_4 served as electrolyte, a Pt wire as CE, and for the RE a Cu|$CuSO_4$ electrode was used, so as to avoid chloride contamination from the Ag|AgCl electrode which would otherwise have been used. When measuring the area of one of the glass electrodes, the potential was first held at 0 V for 5 s, then at 1.4 V for 5 s to form the oxide layer. Then, the potential was swept back to 0 V at a scan rate of 0.1 V/s to reduce the oxide. This results in a reduction peak around 0.8 V, and the integration of this peak current with respect to time gives the electric charge associated with the reduction. This value is then divided by the charge density associated with a monolayer of gold oxide (386 $\mu C/cm^2$ real area [16], [17]) to give the real surface area.

The same setup was used to measure the surface areas of two of the pulled electrodes, one nanoporous and one with an unmodified surface. The difference in this case was that multicyclic CV was carried out instead of holding the potential and then sweeping once. This was done as a surface cleaning procedure, but the data can be used for surface area calculation as well, since the same reduction peak is present.

3.2.5 NPG formation by alloying/dealloying

The protocol for creating NPG electrodes by alloying/dealloying was adapted from the one used by Jia et al. [8] Anhydrous $ZnCl_2$ ($\geq$ 99%, Sigma-Aldrich, USA) was dissolved in benzyl alcohol ($\geq$ 99%, Sigma-Aldrich, USA) at 60°C to yield a 1.6 M solution. 12 ml of this was used per session. A Zn plate was used as CE, with an area roughly 1x1 cm in size immersed in the electrolyte, and a piece of Zn wire served as RE. The CE and RE were sanded with P240 sandpaper immediately prior to use. The solution was heated to 90-120°C with a hot plate in a silicone oil bath, and a 0.5 cm layer of oil was added on top of the electrolyte to prevent evaporation. The alloying and dealloying was achieved by CV, with the number of cycles varying between experiments to find an optimum. The lower potential limit was set to -0.72 V, and the upper limit to 1.88 V. The first cycle started at the open circuit potential, which was determined to be roughly 0.8 V, then the potential was swept to the lower limit, and then to the upper limit. Subsequent cycles ran between

these limits. No Faraday cage was used for this procedure. When the procedure was over, electrodes were cleaned immersion in benzyl alcohol, acetone, isopropanol, ethanol, and deionized water, in that order.

3.2.6 NPG formation by anodization

Another method for the creation of a nanoporous layer on a gold electrode was described by Sukeri et al. [7] and requires no sacrificial metal or elevated temperatures. The gold electrode was immersed in 0.5 M H_2SO_4 along with an Cu|$CuSO_4$ RE and a Pt wire CE. The potential was swept from 0 to 2.0 V at a scan rate of 0.02 V/s, after which the potential was held at 2.0 V for a time before being swept back to 0 at the same rate. During the hold time the gold electrode is anodized as an oxide layer is formed, and this oxide layer is then reduced during the reverse scan, leaving behind a porous structure. Two different hold times were tested, 10 and 60 min.

3.3 Surface characterization by SEM

The morphology and geometric area of the pulled glass encased electrode surfaces were analyzed using a JEOL 7800F Prime scanning electron microscope (JEOL Ltd., Japan). The silver wires of the electrodes were grounded with copper tape to prevent charge build-up in the electrode during imaging. The same instrument was also used for EDX analysis.

4 Results and discussion

4.1 Plastic electrodes

The fabrication and testing of these electrodes served as practice in preparation for the electrodes made with glass capillaries, and as such only three were made in a single batch. CVs were recorded before and after electrochemical cleaning of their surface, as well as before and after cutting the exposed gold wire to examine the effect of minimizing the active area. A representative CV recorded before and after the surface cleaning treatment is shown in figure 9. As the figure shows, cleaning the surface causes slight changes in the CV response, but not in any clearly predictable way. These CVs also showed characteristic, noisy and irregular peaks in the lower potential range, which detract from the textbook duck shape of the voltammogram. The cause of these peaks was not established, but they were found to be related to the size of the active area, as the cutting tests described below show.

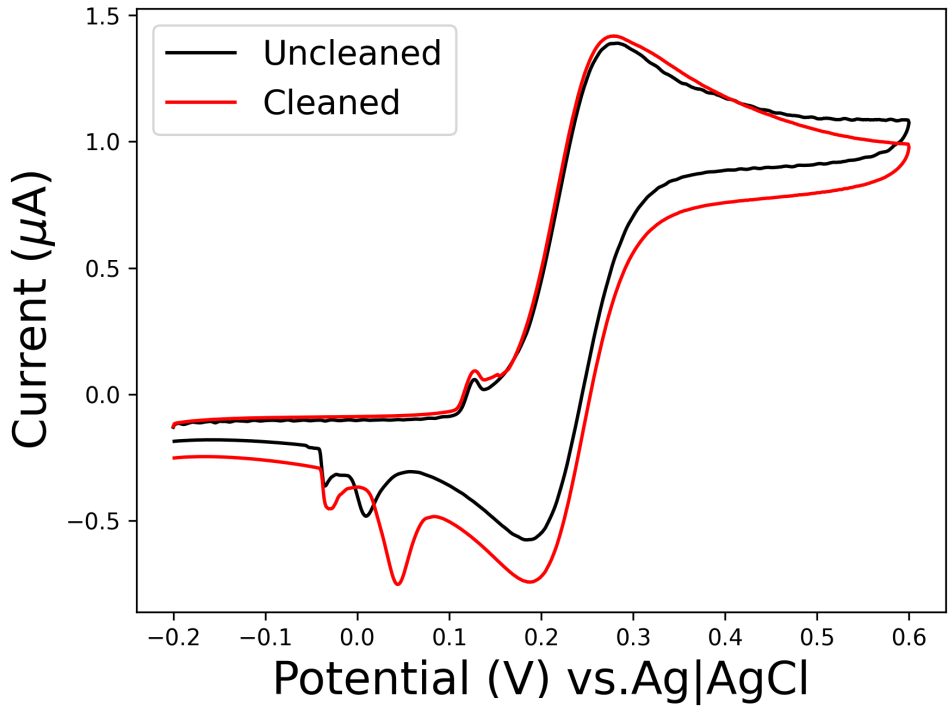

Figure 9: CV in 1 mM FcMeOH and 100 mM KCl before and after cleaning one of the three plastic electrodes.

Cutting tests were performed by gradually cutting the exposed gold wire and performing CV measurements after each cut. CVs were recorded in 10 mM PBS to exclude the possibility of the unknown peaks being caused by ferrocenemethanol. Representative results from the cutting tests are shown in figure 10. Here, cuts are followed by a decrease in current, since the electrode-electrolyte interface is smaller and therefore has a lower capacity for charge exchange. One electrode showed the opposite behavior, where peak currents went from roughly 25 nA to 0.7-4.7 µA (not shown).

Because of this, this electrode was considered defective and was discarded. Another important feature of the voltammogram in figure 10 is that the unknown peaks toward the lower potential range disappear when more cuts are made, as alluded to earlier.

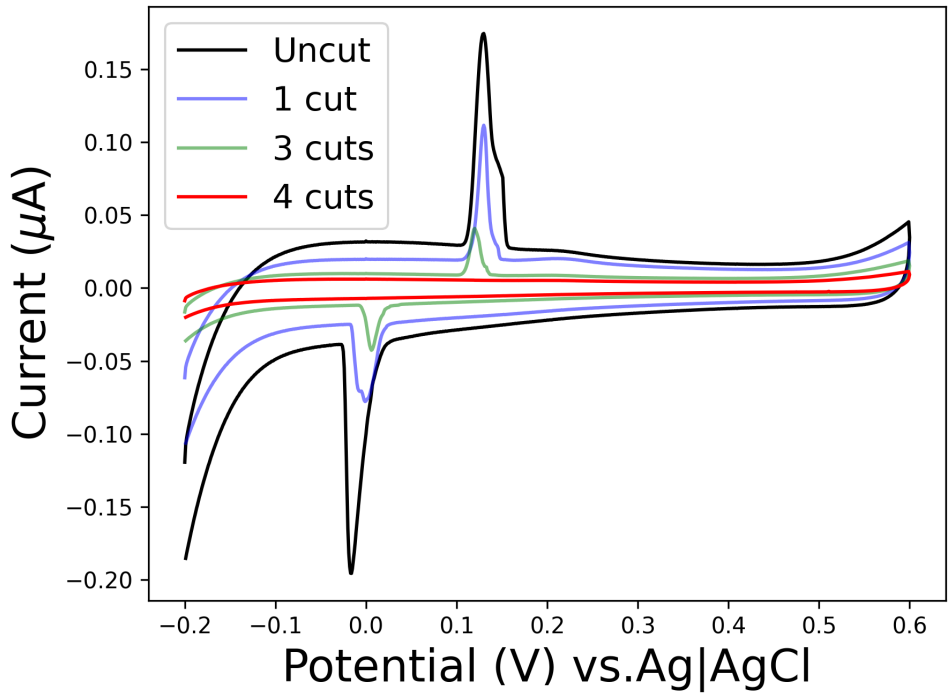

Figure 10: CV in 10 mM PBS before and after cutting one of the three plastic electrodes a number of times.

After the usable electrodes were cut, their responses in ferrocenemethanol were also recorded, and the results for one of these are shown in figure 11, as compared with its original voltammogram. Just like the voltammograms recorded in PBS, these recordings showed that minimizing the electrode surface area decreased the overall current and removed the unknown peaks. These peaks could be caused by interference from the chloride ions in solution, but this would need to be confirmed by testing the electrodes in a chloride-free electrolyte. It was also hypothesized that these peaks could be caused by silver ions leaking from the RE and interfering with the gold surface, but this idea was discarded after experiments were conducted with a salt bridge setup. The salt bridge experiments are detailed in section 4.2.1.

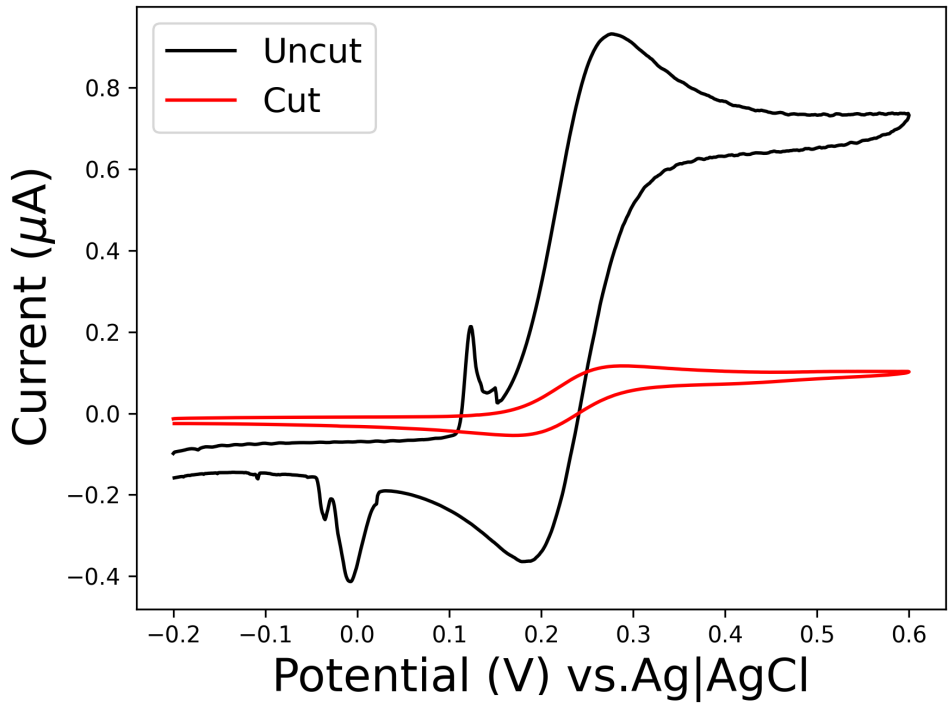

Figure 11: CV in 1 mM FcMeOH and 100 mM KCl before and after cutting one of the plastic electrodes.

4.2 Glass electrodes

The CV responses of some of the electrodes from the first batch of glass electrodes are shown in figure 12. Figure 12a shows examples of acceptable responses. There was some variability in the amplitude of the current, but they were all in the expected low microampere range, and the characteristic duck shape was shown in all cases, along with the unknown peaks in the lower potential range. The variability in current amplitude can be explained by the fact that precisely controlling the amount of gold wire protruding is not possible with this fabrication method, leading to a relatively large variability in active surface area. In contrast, the voltammograms in figure 12b show some typical signs of defective electrodes. Electrodes 6 and 8 almost exhibited the correct shape, but there was an extra plateau at the high end of the potential range, and electrode 8 showed particularly large unknown peaks. The voltammogram for electrode 7 had an almost linear shape, formed by a very noisy current in the nanoampere range. These voltammograms exemplify how CV can be used as a quality control.

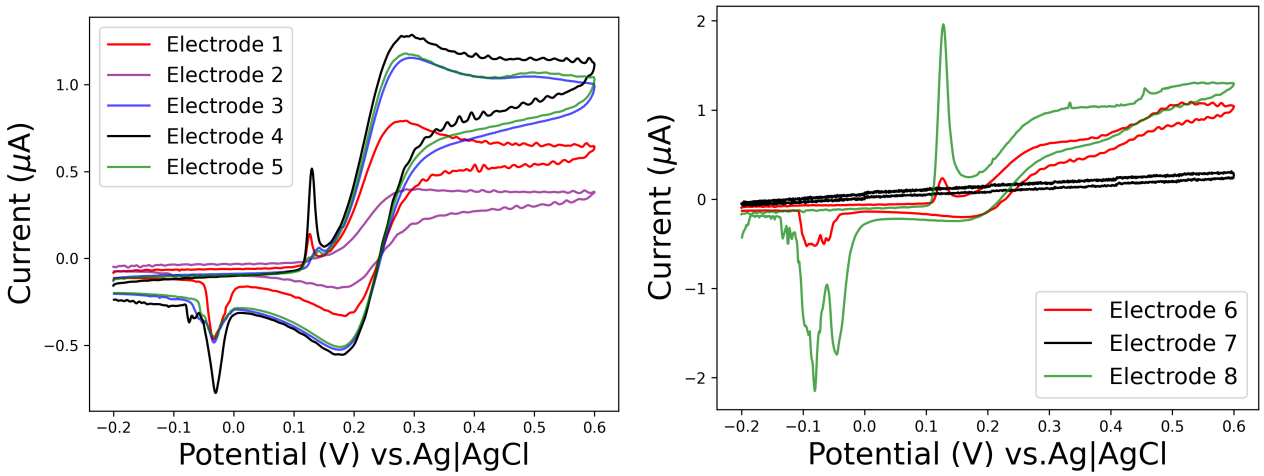

(a) Examples of good initial CV responses.

(b) Examples of bad initial CV responses.

Figure 12: CV in 1 mM FcMeOH and 100 mM KCl for some of the glass electrodes.

4.2.1 The effect of potential range and salt bridge on the unknown peaks

To examine if the unknown CV peaks were caused by leakage of silver ions from the RE and interfering with the WE, the electrochemical cell was separated into two half cells, connected with a salt bridge. The salt bridge was made from a rigid plastic filter, cut to an appropriate shape and soaked in KCl solution. For the first measurement the filter was soaked in 100 mM KCl, but this proved to be too low a concentration for the circuit to complete, so it was then soaked in 1 M KCl. The Pt wire CE was placed in the same half cell as the Ag|AgCl RE, as seen in figure 13. Both half cells were filled with 1 mM ferrocenemethanol and 100 mM KCl, the scan rate was 0.1 V/s, and the potential limits were -0.2 V - 0.6 V. A representative result from the salt bridge tests is shown in figure 14. Evidently, the unknown peaks were not caused by silver ions, nor platinum ions from the CE, since the peaks were also present in these voltammograms.

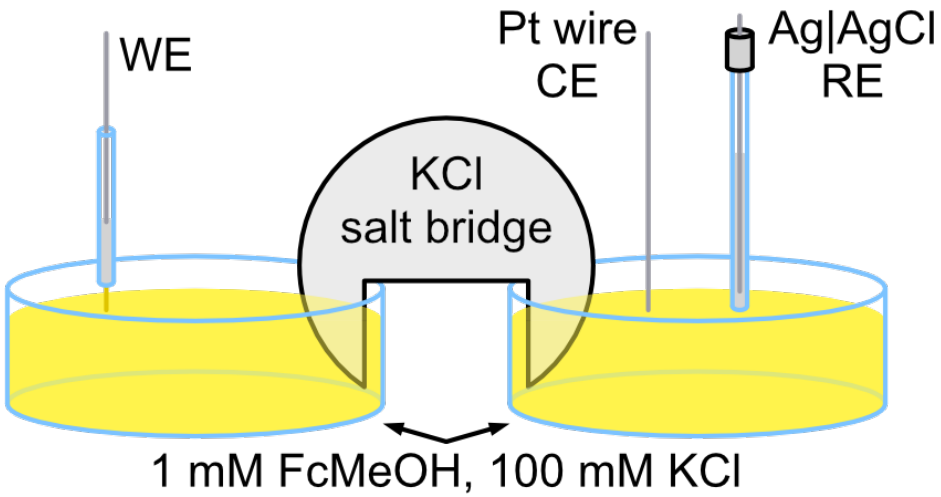

Figure 13: Illustration of the setup for the salt bridge tests.

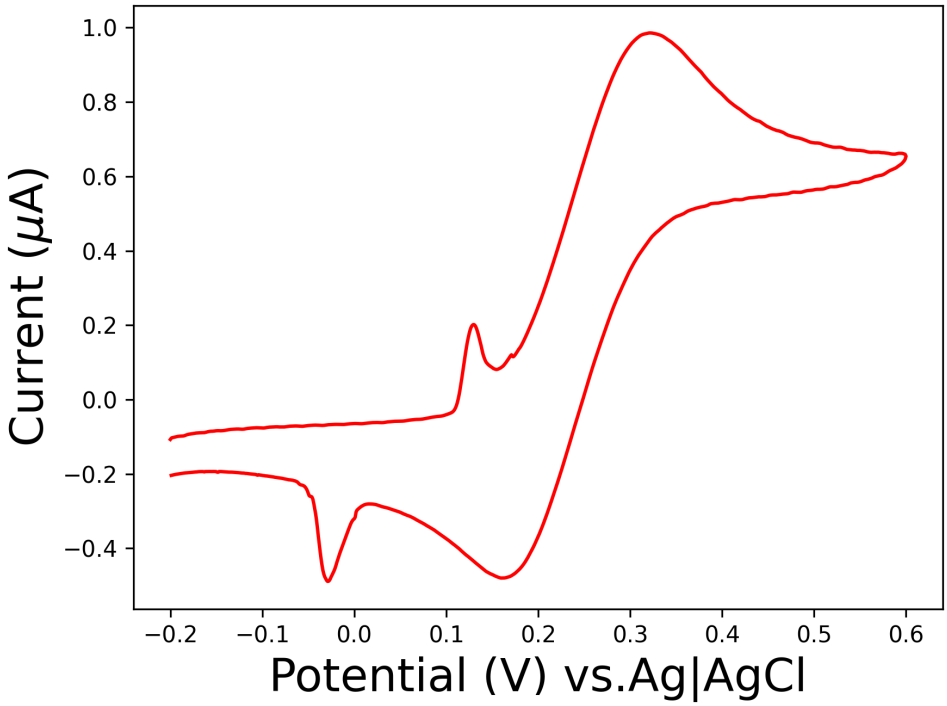

Figure 14: A representative CV recorded with the salt bridge setup.

The potential range was also adjusted to see how this would affect the peaks. The lower potential limit was incrementally increased from -0.2 V to 0.05 V, while the upper limit was left unchanged. This meant that the cathodic peak would eventually be out of range, but the anodic peak appeared around 0.13 V, and would therefore be in range for every measurement. These experiments were performed without a salt bridge, and a representative example of how the voltammogram changed is shown in figure 15.

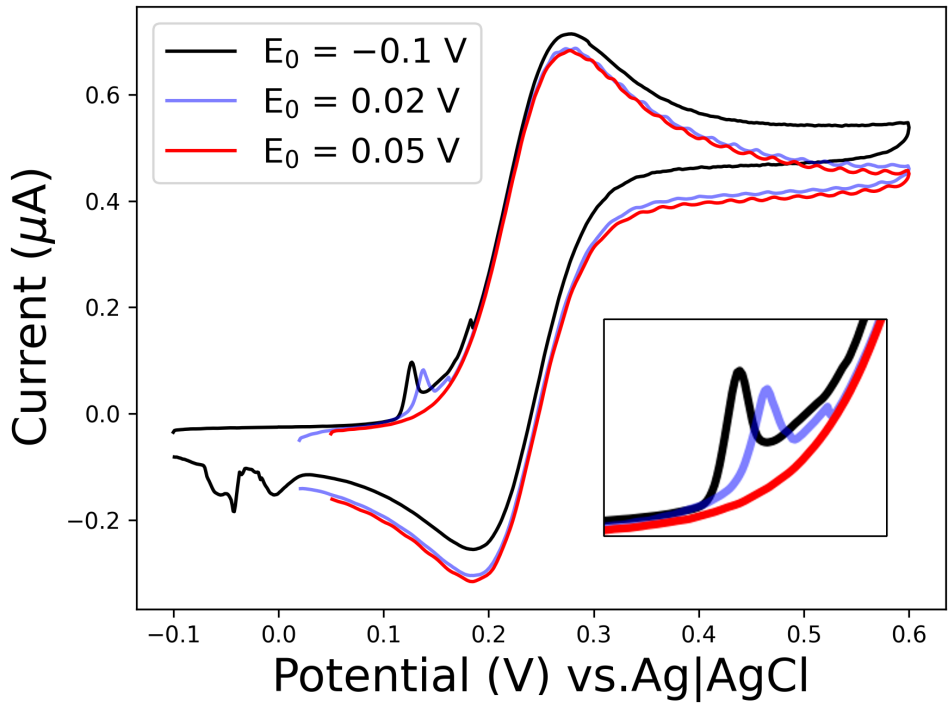

Figure 15: Repeated CVs in 1 mM ferrocenemethanol, 100 mM KCl *vs* Ag|AgCl for a glass electrode, each cycle having a higher initial potential than the last. Inset: a zoomed-in view of the unknown anodic peak.

Five glass electrodes were tested in this way, and the same pattern held for each: the unknown anodic peak around 0.13 V disappeared once the lower potential limit was raised to 0.05 V. The cause of the peaks remained unknown, but since they tended to disappear when the surface area was small enough, as the results for the pulled electrodes show in sections 4.3.1 and 4.4, this issue was not considered further. The peaks might be caused by interference from chloride ions, and this could be confirmed or refuted by performing further experiments in a chloride-free solution.

4.2.2 Surface area measurements

The surface area of one of the electrodes was measured electrochemically and the result was compared with its estimated geometric area. The latter was estimated by measuring the length of the exposed gold wire, roughly 4.5 mm, and using this together with the known diameter of the wire to calculate the area of a cylinder having those dimensions, minus one of the circular faces, since only one end of the wire was exposed. This resulted in a geometric area of 0.35 mm^2. The real area was measured according to the procedure described in section 3.2.4, which resulted in a real area of 0.37 mm^2, and thus a roughness factor of about 1.06. This is an expected result, since no surface modifications had been made, meaning the surface was relatively smooth. Thus, the real and geometric areas are expected to be similar, the former only having a slightly larger value than the latter. The voltammogram used to acquire the real surface area can be found in the appendix. The following sections detail how the surface areas were insulated in an attempt to minimize and control them.

4.2.3 Insulation method #1: epoxy + paraffin wax

Epoxy resin and hardener were thoroughly mixed 4:1 before three electrodes were immersed for 20 min. Then, they were allowed to cure in an oven at 100°C overnight. The CVs recorded the next day, an example of which seen in figure 16a, showed that the epoxy was only partially able to insulate the gold, so more coats were applied. These extra coats were applied by heating the epoxy resin to 50°C and dipping the electrodes for 5 s, then partially curing the coating by placing the electrodes in the oven at the same temperature for 5 min. By applying the extra coats in this way rather than immersing them for 20 min at room temperature, it was hoped that the epoxy would more easily wet the surface. Additional coats were to be added 10 times, but after 7 coats it was noticed that the epoxy formed larger and larger beads instead of fully wetting the wire, so the procedure was interrupted and the electrodes were left overnight in the oven at 100°C to completely cure the epoxy. This did not complete the insulation either, so as a final attempt, paraffin wax was melted on a hot plate and the electrodes were dipped in this for 5 s and then left to dry at room temperature overnight. As figure 16b shows, the insulation was still incomplete.

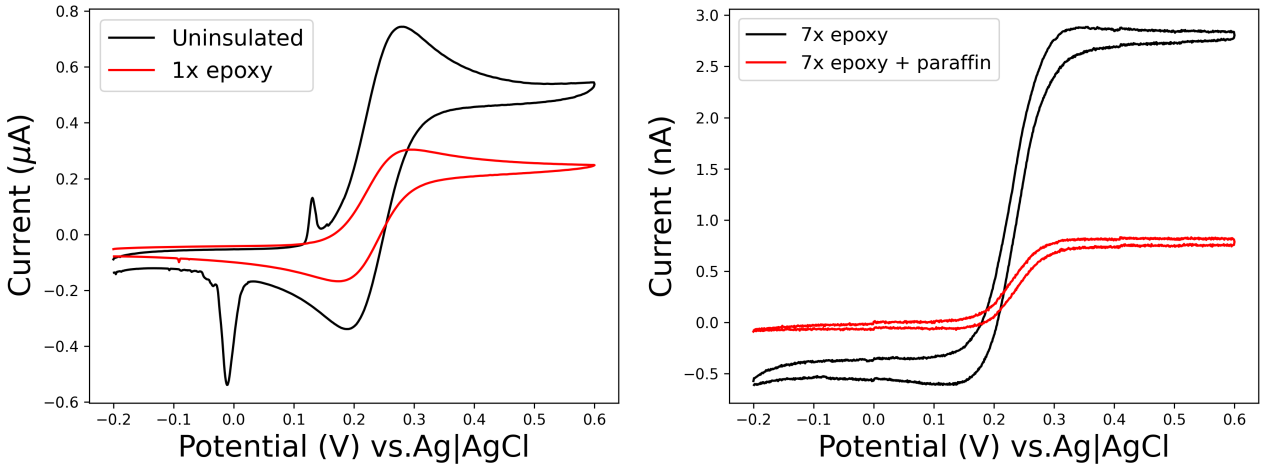

(a) Before and after one epoxy coating.

(b) After several epoxy and paraffin coatings.

Figure 16: CV in 1 mM FcMeOH and 100 mM KCl for a glass electrode after epoxy and paraffin coatings.

An interesting effect of the incomplete insulation is that the duck shape of the voltammogram, seen clearly in figure 16a, was flattened out to the point where the oxidation and reduction peaks more closely resembled plateaus, as figure 16b shows. As sections 4.3.1 and 4.4 will show, this is a consistent result of minimizing the surface area of the electrode, which partial insulation is an example of. The peaks in the voltammogram appear for the following reason: during the positive potential sweep, analytes move to the electrode and become oxidized, and after this happens, the oxidized species must move away from the electrode if more analyte molecules are to undergo the reaction, since they would otherwise be in the way. At the oxidation peak, the electrolyte layer around the electrode surface is temporarily depleted of unoxidized molecules, and the current is limited by the rate at which more analyte molecules can diffuse through this layer of oxidized molecules, called the diffusion layer. This causes the current to decrease in amplitude somewhat.

The systematic absence of this feature in voltammograms recorded with electrodes with smaller surface areas is a consequence of the electrode size and disc-shape. These factors make the diffusion layer hemispherical, allowing electroactive molecules to approach the electrode surface from the side rather than head-on, which they are forced to do when the surface is larger and the diffusion layer has a semi-infinite linear profile [18].

4.2.4 Insulation method #2: phenol, 2-allylphenol copolymer + epoxy

The phenol, 2-allylphenol copolymer base coat was formed *via* electropolymerization, an insulation method used with success by Strein and Ewing for carbon electrodes [19]. A solution of 60 mM phenol ($\geq$ 99.5%, Sigma-Aldrich, USA), 90 mM 2-allylphenol ($\geq$ 98%, Sigma-Aldrich, USA) and 2% 2-butoxyethanol ($\geq$ 99%, Sigma-Aldrich, USA) was prepared in a 1:1 mixture of deionized water and methanol ($\geq$ 99%, Sigma-Aldrich, USA). The pH of the solution was then adjusted to 9 by adding 5 M NaOH, followed by 1 M HCl due to a slight overshoot. Gold electrodes were immersed in this solution together with a Pt wire CE/RE, and a potential of 4.0 V was applied for 30 min. This caused the phenol and 2-allylphenol to copolymerize at the WE surface, forming a thin, black film. It was noticed that the film was not uniform, and some parts of the gold wire still showed a metallic shine. The polymer was then cured by placing the electrodes in an oven at 150°C for 30 min. Following this, the electrodes were immersed in epoxy resin three times, for 1 min each time, before the epoxy was cured in an oven at 100°C overnight. This was repeated three times to form three epoxy coatings, and the CV responses after each coating is seen in figure 17. The initial copolymer coating resulted in better insulation than epoxy applied directly to the gold surface, but it was still incomplete, and subsequent epoxy coatings could not complete the insulation.

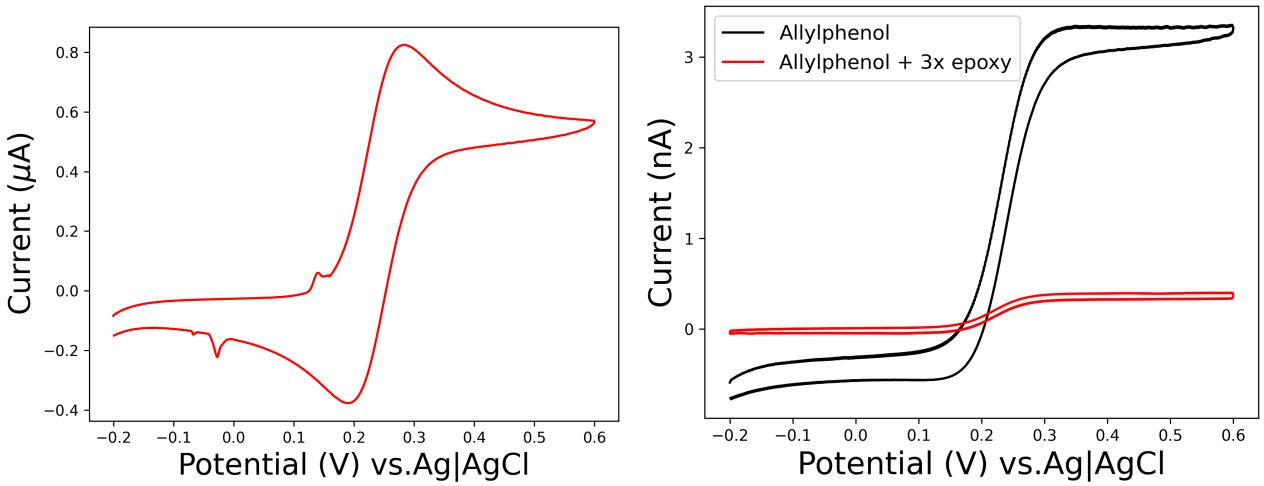

(a) Before attempted insulation.

(b) After attempted insulation.

Figure 17: CV in 1 mM FcMeOH and 100 mM KCl for a glass electrode after phenol-allylphenol copolymer and epoxy coatings.

4.2.5 Insulation method #3: Nafion™ + epoxy

Electrodes were first dipped in Nafion™ dispersion D520CS (Ion Power, GmbH, Germany) for 5 min before being left to dry overnight at room temperature. As with the other two methods, this did not result in complete insulation, so epoxy coatings were then applied. The electrodes were immersed in epoxy resin three times, for 1 min at a time, before being cured in an oven at 100°C overnight. When this did not achieve complete insulation either, more epoxy coats were applied in the same manner as before. Three epoxy coats were applied, but insulation was still incomplete, and due to epoxy beading, this method was considered unviable like the others. CVs recorded with the one of the electrodes before and after the insulation coatings were applied are shown in figure 18.

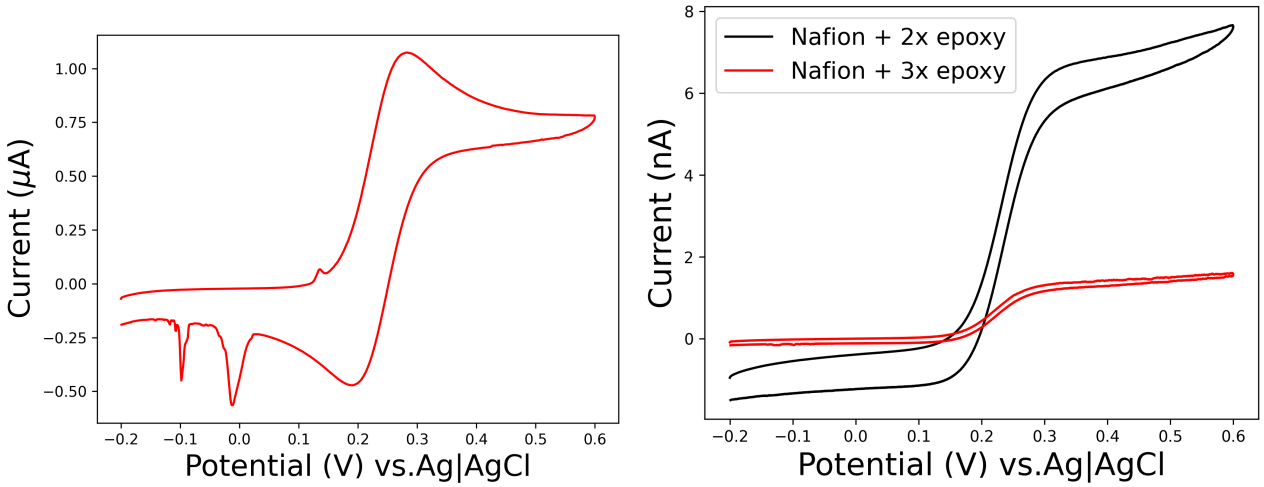

(a) Before attempted insulation.

(b) After attempted insulation.

Figure 18: CV in 1 mM FcMeOH and 100 mM KCl for a glass electrode before and after Nafion™ and epoxy coatings.

4.2.6 NPG formation by dealloying

Two electrodes were cycled 10 times in the dealloying solution at 120°C. No silicone oil was used to prevent solvent evaporation or as a bath for the electrochemical cell, since this was not mentioned in the article by Jia et al. [8], and was only used in later attempts with pulled glass encased electrodes after realizing that Downs et al. used this method in their procedure [9]. SEM images of the glass electrodes are shown in figure 19. Though some vaguely nanoporous structures can be seen to the right in figure 19a, NPG formation was clearly unsuccessful.

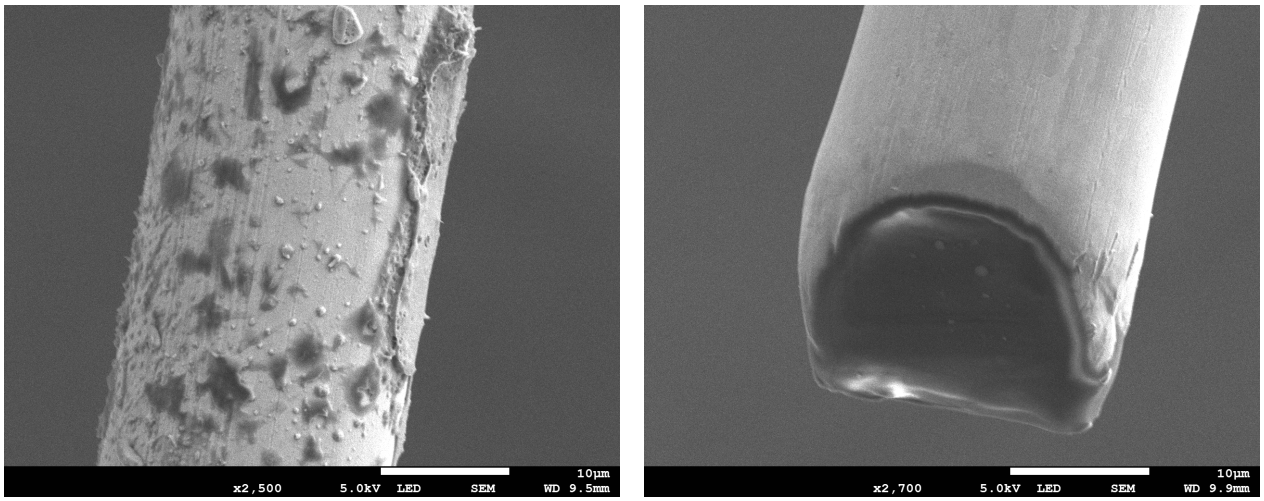

(a) (b)

Figure 19: SEM images of one of the failed dealloyed NPG electrodes.

4.2.7 NPG formation by anodization

Two electrodes were given the anodization treatment. One was oxidized for 10 min and the other for 60 min. Sukeri et al. reported that their gold electrodes turned a black color after the NPG formation [7], but this was not observed here. As the SEM images seen in figure 20 show, no NPG layer was formed on the electrodes.

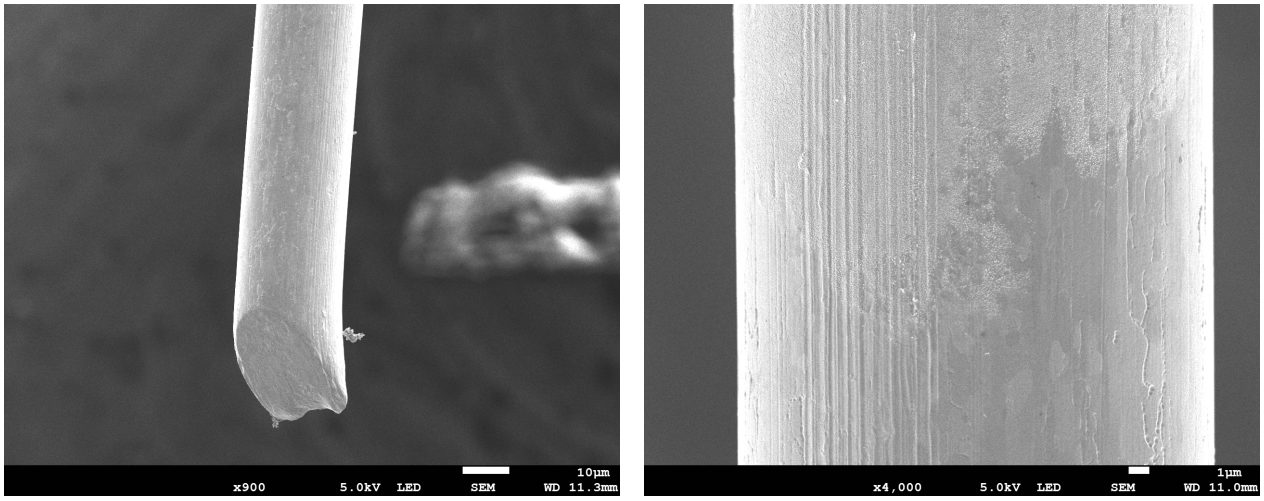

(a) (b)

Figure 20: SEM images of one of the failed anodized NPG electrodes.

4.3 Pulled glass encased electrodes (P-1000)

There are five parameters that can be set to affect how the puller carries out its action. The Heat parameter controls the temperature of the heating filament, Pull controls the force of the pulling action, Velocity controls the velocity of the pull, Time determines how long the air cooling is active for, and Pressure controls the air pressure during the cooling. A few different settings were tried, but most gave poor or inconsistent results. One combination was discovered that reliably gave some interesting results, as described below in section 4.3.1, but after a few pulls the results changed, and it was concluded that this probably was the result of a malfunction of the machine, prompting the switch to the P-2000 model puller.

4.3.1 Nanotip electrodes

As previously alluded to, during the optimization of the settings of the micropipette puller, a combination was discovered that seemingly reliably produced nanotip electrodes each run. These electrodes had a few micrometers of exposed gold wire at the tip which was conical in shape and severely compressed from its original 25 µm diameter. SEM images of these tips are shown in figure 21. At the glass edge the diameter of the capillary was between 3.2-3.6 µm, and the diameter of the gold wire was between 1.1-1.5 µm. Six nanotip electrodes were produced before the puller supposedly malfunctioned, three of which contained intact gold wires. The settings that gave rise to these electrodes were as follows: Heat = 533, Pull = 100, Velocity = 13, Time = 250, Pressure = 500. The numbers themselves are unitless and relative to the capabilities of the instrument.

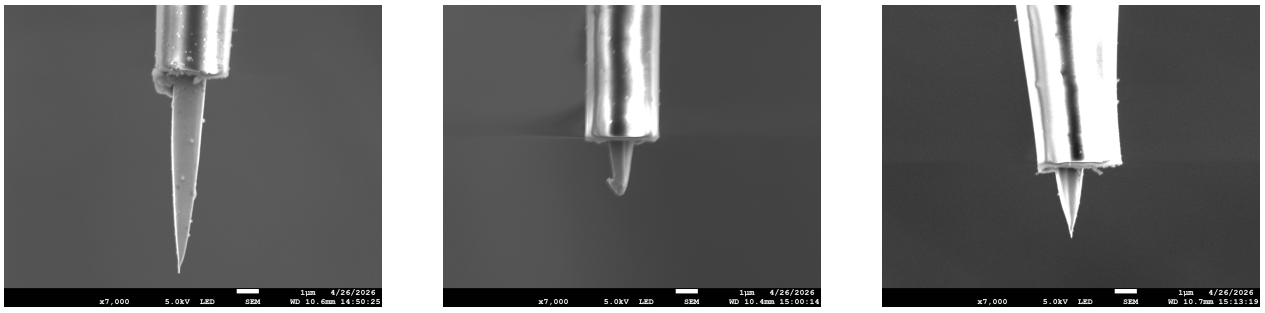

(a) Nanotip 1 (b) Nanotip 2 (c) Nanotip 3

Figure 21: SEM images of the three nanotip electrodes. Scale bar = 1 µm.

CV responses in ferrocenemethanol for the three nanotip electrodes are shown in figure 22. They are fairly duck shaped, albeit slanted, and unexpectedly bloated in the case of nanotip 3. The current amplitudes were similar, all in the nanoampere range, and no unwanted peaks were present. This type of electrode is also of great interest in neuroscience, and if these results are reproducible with a P-1000 puller functioning as intended, it could potentially be a very useful new method of producing them, since a simple, one-step fabrication method for gold nanotip electrodes does not yet exist to the best of the author's knowledge. However, the main focus of this project was to produce the type of beveled electrodes described in section 3.1.3, so further testing of the nanotip electrodes was not pursued.

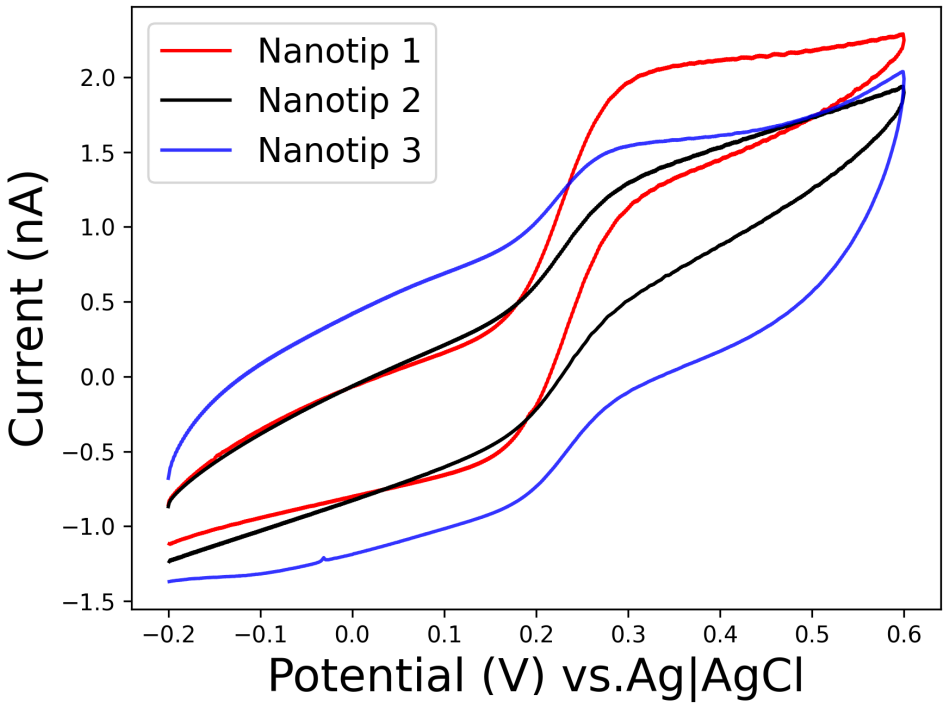

Figure 22: CV responses of the three gold nanotip electrodes in 1 mM FcMeOH and 100 mM KCl.

4.4 Pulled glass encased electrodes (P-2000)

Velmurugan, Sun and Mirkin used this model of micropipette puller to fabricate gold nanoelectrodes [20], but they did not explicitly state all of the parameter settings they used, instead referring to previous works. The rest of the settings could not easily be found in these reports, however [21], [22], [23], so only the settings for the heat and velocity parameters could be reproduced, while the rest of the parameters were set based on settings that were used to make carbon fiber electrodes in our lab. The plan was to use these settings as a starting point and then optimize them based on the results, since there are substantial differences in material properties between carbon fiber and gold, but the combination could surprisingly reliably yield usable gold electrodes, and the settings were kept unchanged throughout the rest of the project. The parameters were set as follows: Heat = 400, Filament = 4, Velocity = 30, Delay = 220, Pull = 100. These parameters control the heating temperature, the length of the capillary that is heated, the velocity of the pull, the delay between heating and pulling, and the strength of the pull, respectively. As in the case of the P-1000 puller, the numbers themselves are relative to the capabilites of the instrument. In total, 44 electrodes were pulled using the settings listed above, and 27 of these were usable, giving a total success rate of roughly 61%.

A representative CV in ferrocenemethanol is shown in figure 23. As expected due to the smaller surface area, the current amplitude was in the nanoampere range, compared with the microampere currents observed with the plastic and glass electrodes. The smaller surface area also had two other

effects on the voltammogram, namely, the unknown peaks in the lower potential range were absent, and the duck shape was more flattened out, such that the oxidation and reduction peak currents were similar to the current amplitudes at the potential limits. As previously discussed, these effects were observed in the case of the plastic and glass electrodes when their active surface areas were minimized.

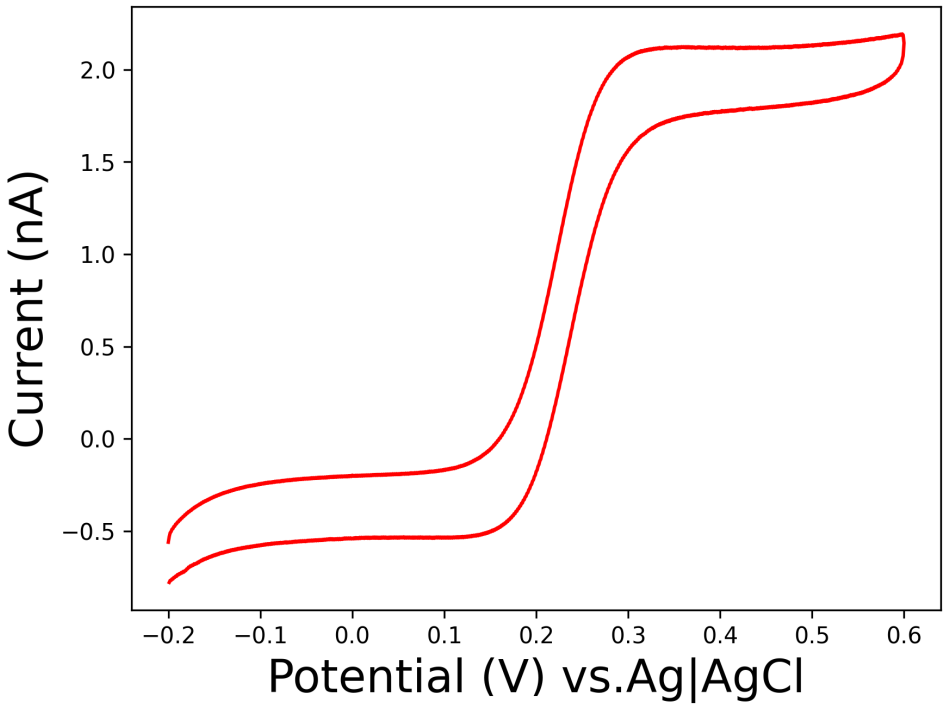

Figure 23: Representative CV of a laser pulled electrode in 1 mM ferrocenemethanol and 100 mM KCl.

An SEM image of one of the pulled glass encased electrodes is shown in figure 24. This image allows for an easy measurement of the geometric surface area by using the scale bar and the equation for the area of an ellipse. This calculation gives a geometric area of roughly 219 μm^2. The image also shows that the diameter of the gold wire was compressed by the pipette puller, only slightly in one direction but rather substantially in the other. Figure 24b shows the roughness of the surface more clearly. This rough texture is a result of the beveling process.

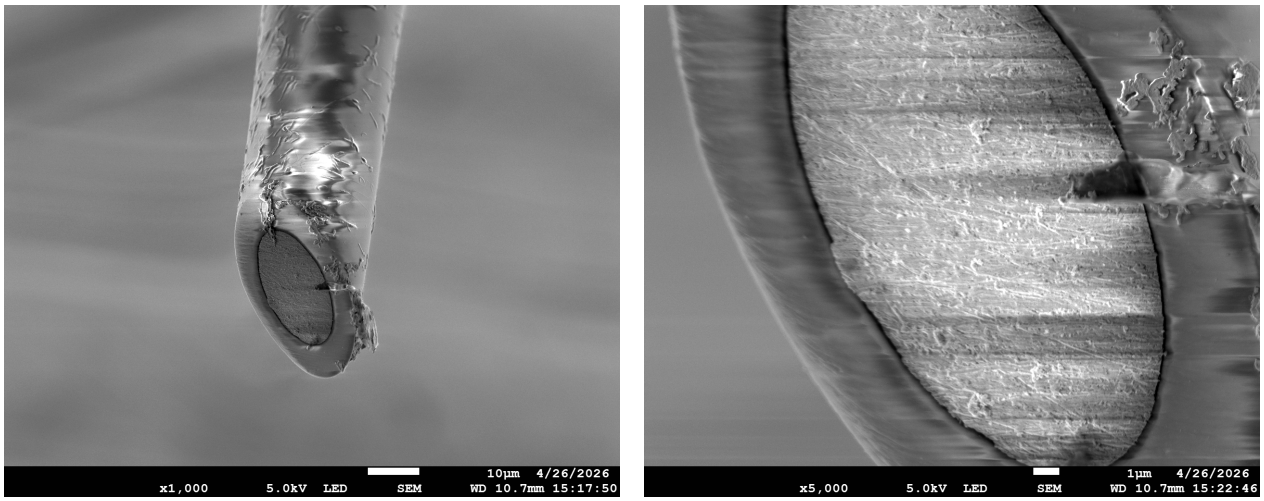

(a) (b)

Figure 24: SEM images of a pulled glass encased electrode. Scale bar = 10 µm (a), and 1 µm (b).

The SEM images of eight of these electrodes were used to estimate their geometric areas, which are tabulated in table 1. Clearly, the area is variable enough that one electrode cannot safely be assumed to have a comparable area to another.

Electrode #	1	2	3	4	5	6	7	8	Average
A_{geo} (μm^2)	219	197	95	88	219	160	197	233	176

Table 1: Geometric areas of six pulled glass encased electrodes, based on SEM images.

4.5 Pulled glass encased (P-2000) NPG electrodes

The dealloying method was attempted with four electrodes, but only one was successful. The first few attempts were made without an oil bath or any oil on top of the electrolyte, and the temperature of the electrolyte was only measured with an IR gun, which was deemed too inaccurate. At the end of these runs, some of the electrolyte had evaporated, and the electrolyte had taken on a darker color than it had at the start. The number of potential cycles in the first attempts was 30. SEM images of one such electrode are shown in figure 25. Though there were some nanoporous structures at some parts near the interface between the gold and the glass, as seen in figure 25b, most of the surface was homogeneous. The reason for this might be that the current density is greater at the edges of such small, disc-shaped electrodes, so that dealloying started at the edges but was unable to continue over the rest of the surface [18]. These images would then be a visualization of the edge-effects discussed previously to explain the flattened shape of CVs recorded with microelectrodes in section 4.2.3. Further, the surface was smoother than before, as compared with figure 24b. This indicated that there was some surface reconstruction taking place during the dealloying attempt. A contributing factor to this could be the high temperature allowing the surface atoms to more easily reorganize to lower coordination positions.

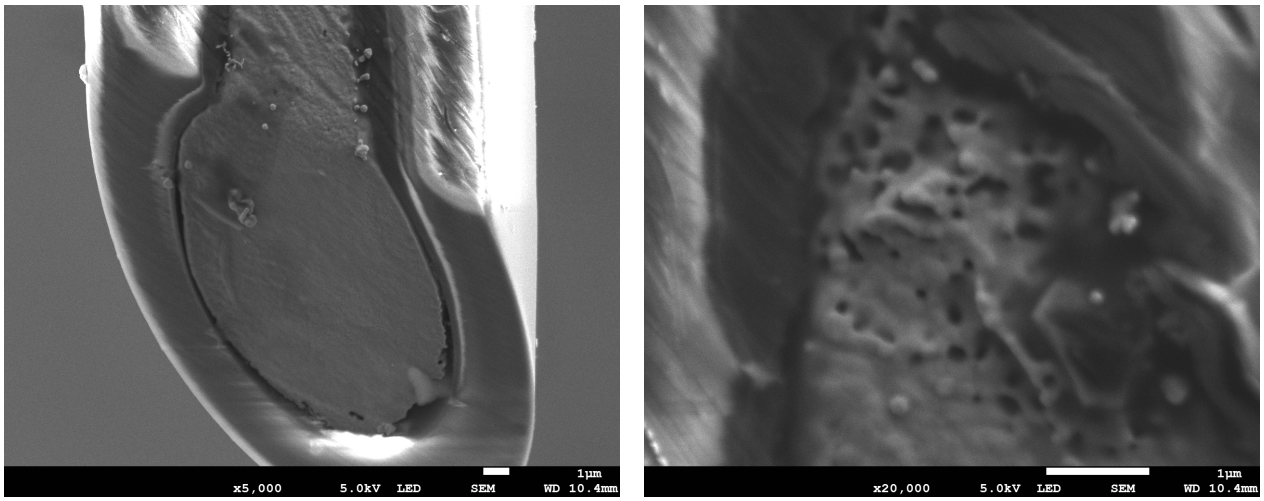

(a) (b)

Figure 25: SEM images of a failed NPG electrode. Scale bars = 1 µm.

The setup was adjusted by including the silicone oil, reducing the number of cycles, and by using a thermometer that continuously measured the temperature of the oil bath. After these changes were made, the next attempt resulted in one NPG electrode, clearly showed by the SEM images in figure 26. The glass had cracked slightly very near the tip, but remained intact further away. The ligaments and pores mostly had diameters slightly larger than 100 nm. In this experiment, the potential was swept for 10 cycles and the temperature was set to 120°C.

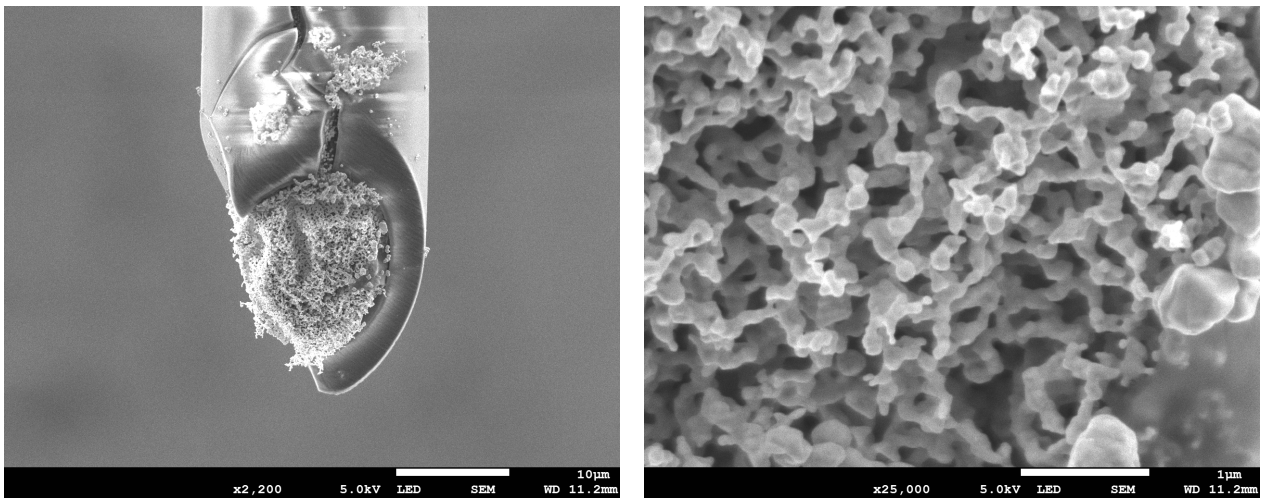

(a) (b)

Figure 26: SEM images of the successful NPG electrode. Scale bars = 10 µm (a), and 1 µm (b).

The experiment was attempted again, but without success. It was realized that the temperature was

accidentally changed at the start of the experiment that gave the NPG electrode, so that it spent a substantial amount of time at temperatures lower than 120°C. To try to replicate these conditions, following experiments were conducted at 90°C instead, but results were still lacking. SEM images of these electrodes are seen in figure 27. In these cases, it appeared that the gold surfaces were covered by some other material. EDX analysis of the electrode shown in figure 25a showed strong signals from carbon and oxygen, but not gold. Analysis of the electrode in figure 27b showed no strong signals from the beveled area, possibly due to technical difficulties. A possible explanation for the carbon and oxygen signals is that some of the epoxy that was applied prior to the beveling step was still covering the tip. For the electrode in figure 27a, there might also be diamond particles from the abrasive plate used during beveling adhered to the surface. This may be investigated in future work by inspecting the electrodes with SEM and EDX before the dealloying procedure, which would rule out the possibility of contamination from the dealloying solution. Images from the EDX analysis can be found in the appendix.

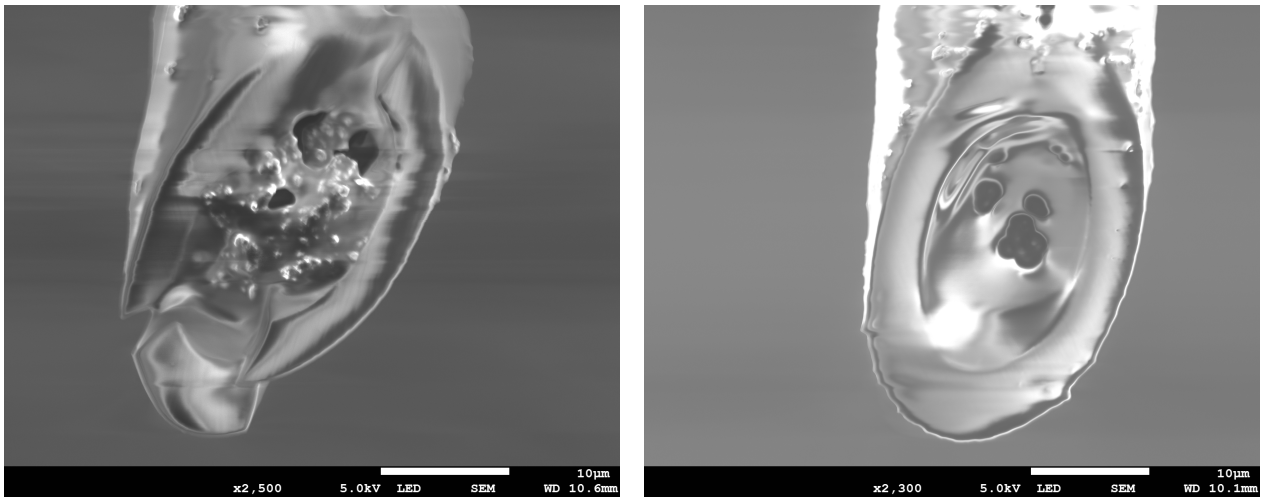

(a) (b)

Figure 27: SEM images of two unsuccessful NPG electrodes. Scale bars = 10 µm

4.5.1 Amperometry

Amperometry was performed for the NPG electrode and one non-NPG electrode for reference. Results recorded at a potential of 0.5 V can be seen in figure 28 and those recorded at 0.8 V are shown in figure 29.

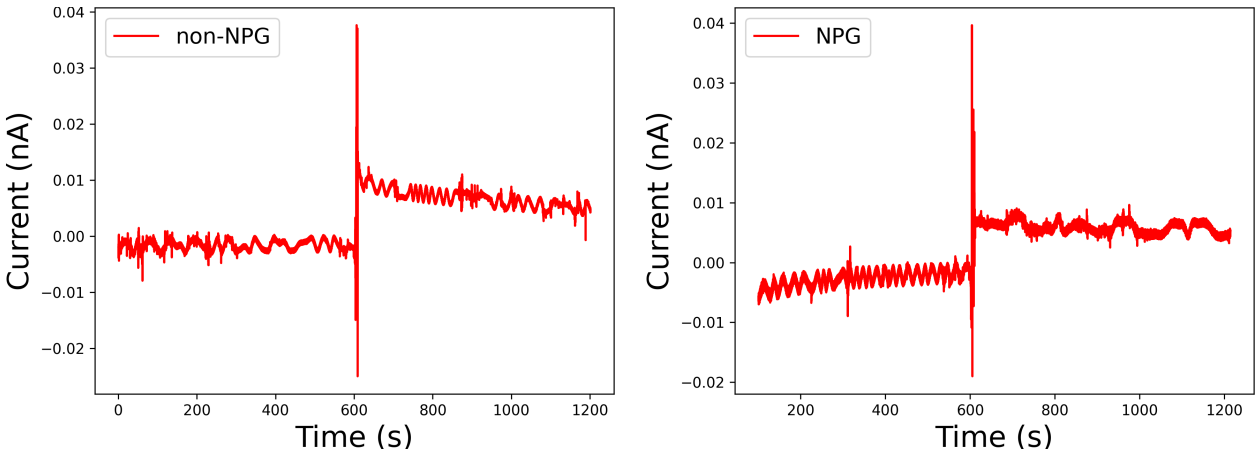

(a) (b)

Figure 28: i-t curves of non-NPG (a) and NPG (b) electrodes at different potentials in 10 mM PBS and 10 mM H_2O_2 at an applied potential of 0.5 V.

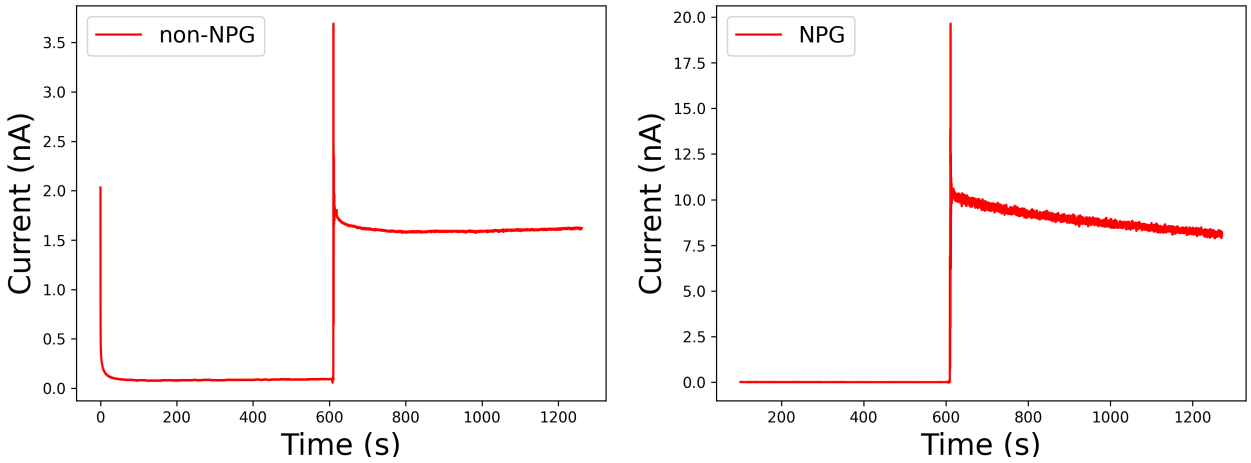

(a) (b)

Figure 29: i-t curves of non-NPG (a) and NPG (b) electrodes at different potentials in 10 mM PBS and 10 mM H_2O_2 at an applied potential of 0.8 V.

Roughly measured current responses are tabulated in table 2. At 0.5 V it was difficult to measure any difference between the responses with accuracy, but at 0.8 V the NPG electrode was unambiguously able to give a signal more than five times as strong as the unmodified electrode. This is a key finding in this study, as it indicates that NPG has the potential to increase the sensitivity of amperometric gold H_2O_2 sensors, which could find applications in studying the initial vesicle-membrane pore formation in the release of neurotransmitters like acetylcholine and glutamate.

Applied potential	$i_{non\text{-}NPG}$	i_{NPG}
0.5 V	8 pA	8 pA
0.8 V	1.5 nA	8 nA

Table 2: Amperometric responses of NPG and non-NPG electrodes at different potentials in 10 mM PBS and 10 mM H_2O_2

4.5.2 Electrolyte effects

CV in ferrocenemethanol was conducted for the NPG electrode, and the resulting voltammogram is shown in figure 30 along with a voltammogram recorded prior to dealloying. The voltammograms were unexpectedly almost identical. The larger surface area that NPG provides should theoretically result in a much larger current.

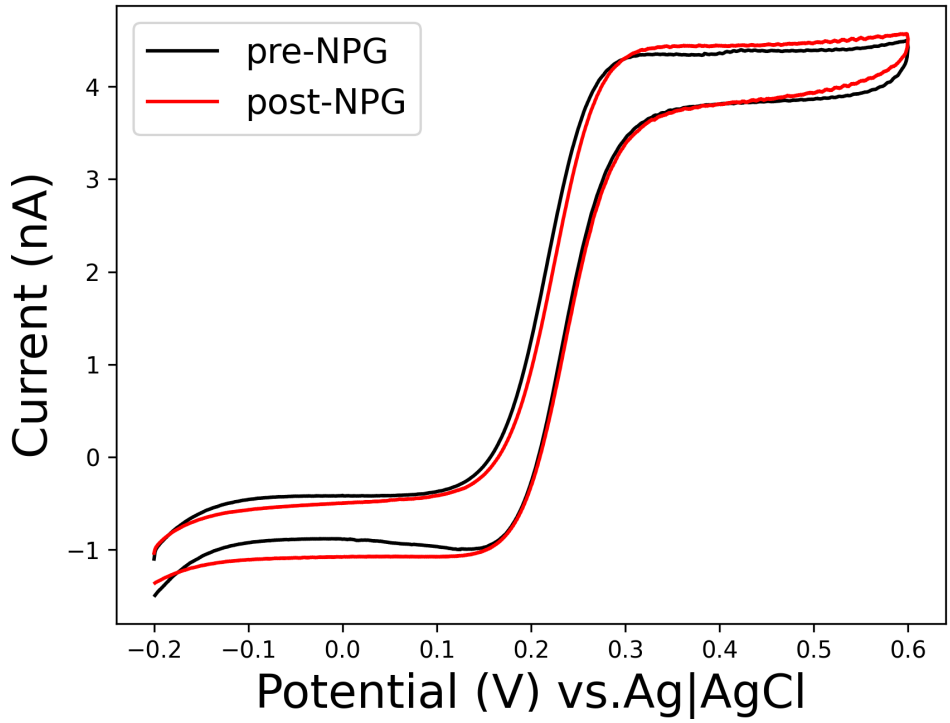

Figure 30: CV in 1 mM ferrocenemethanol and 100 mM KCl, *vs* Ag|AgCl of the NPG electrode prior to and after NPG formation.

Jia et al. [8] used a different electrolyte in their work, namely $[Fe(CN)_6]^{3-/4-}$, so this electrolyte was used to record more voltammograms to see if the results would differ. This was done with the NPG electrode, as well as an unmodified electrode for reference. These CVs were recorded over the same potential interval as previous voltammograms, but with a scan rate of 0.05 V/s and a quiet time of 30 s. The quiet time is a delay at the start of the recording before the potential sweep is initiated. The electrolyte consisted of 5 mM $K_3Fe(CN)_6$ and 0.1 M KCl, and the resulting voltammograms can be seen in figure 31. Here, the results clearly differ between the electrodes,

as the NPG electrode gave rise to a current of roughly twice the amplitude in the lower potential range compared with the non-NPG electrode, as detailed in table 3.

Sweep	$i_{\text{non-NPG}}$ (nA)	i_{NPG} (nA)	$i_{\text{NPG}}/i_{\text{non-NPG}}$
Anodic	-9.787	-22.70	2.32
Cathodic	-11.93	-23.24	1.95

Table 3: Current amplitudes for the non-NPG and NPG electrodes in the CV shown in figure 31, at -0.2 V

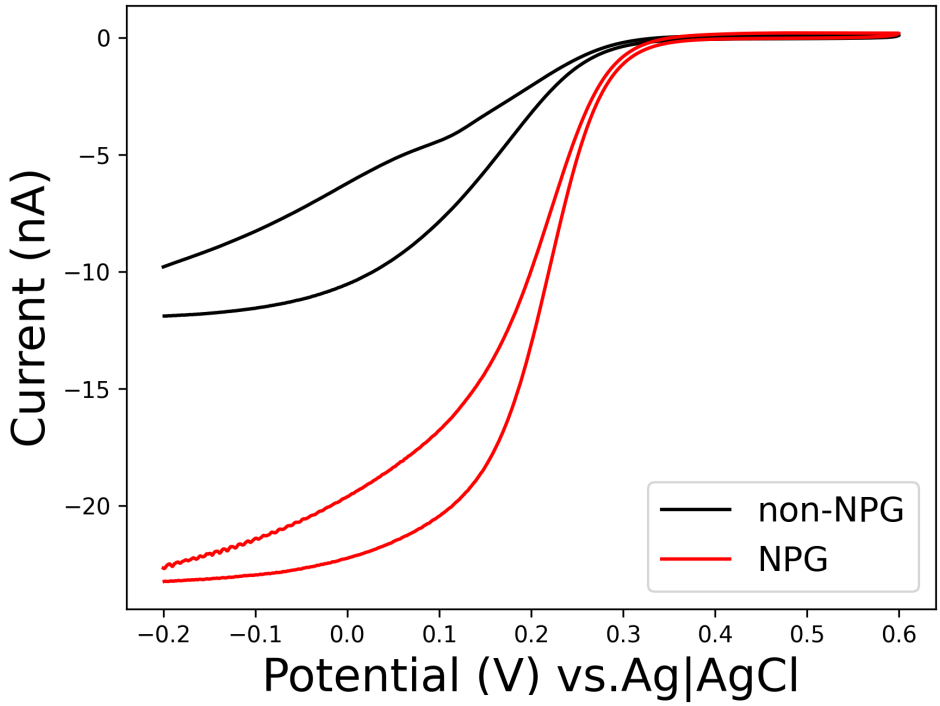

Figure 31: CV recorded in 5 mM $K_3Fe(CN)_6$ and 0.1 M KCl, with the NPG electrode and an unmodified electrode for reference.

Despite the stronger response in the low potential range, the currents were nearly identical in the high potential range. This may be due to how the electrolyte was prepared. The formula for the redox probe, $K_3Fe(CN)_6$, indicates that the anion was in its oxidized state by default, since it is paired with three K^+ cations. Because of this, the redox probe could not undergo further oxidation, leading to a limited anodic current. In contrast, during the cathodic sweep, all of the redox probe molecules could undergo reduction, giving rise to a more dynamic signal.

The question of why the NPG electrode gave an improved signal in $K_3Fe(CN)_6$ but not in ferrocenemethanol can be answered by considering how these redox probes interact with the electrode surface. The terms inner-sphere and outer-sphere are sometimes used to describe redox probes depending on the mechanism of charge transfer with the electrode surface. Outer-sphere probes may

react with the electrode without coming into direct contact with it, as there is a layer of solvent molecules separating them [24]. In contrast, inner-sphere probes make direct contact with the electrode surface when the charge transfer occurs. Ferrocenemethanol is an outer-sphere redox probe, whereas $[Fe(CN)_6]^{3-/4-}$ is often described as an inner-sphere probe [25], [26], though it has been described as outer-sphere as well [24]. Its behavior is complex and beyond the scope of this thesis, but the important difference in this case between the two redox probes is that $[Fe(CN)_6]^{3-/4-}$ is more sensitive to the surface morphology of the electrode, which explains the difference seen in the voltammograms in figures 30 and 31.

Other than CV, SWV was also performed for the two electrodes. This was done in 5 mM $K_3Fe(CN)_6$ and 0.1 M KCl between −0.5 V and 0.7 V with increments of 4 mV, a frequency of 10 Hz, and an amplitude of 25 mV. The results are seen in figure 32. Here it can be seen once again that the NPG electrode is more sensitive to the redox probe than its non-NPG counterpart. The peak is also shifted to lower potential values. The cause of this or its implications have not yet been established.

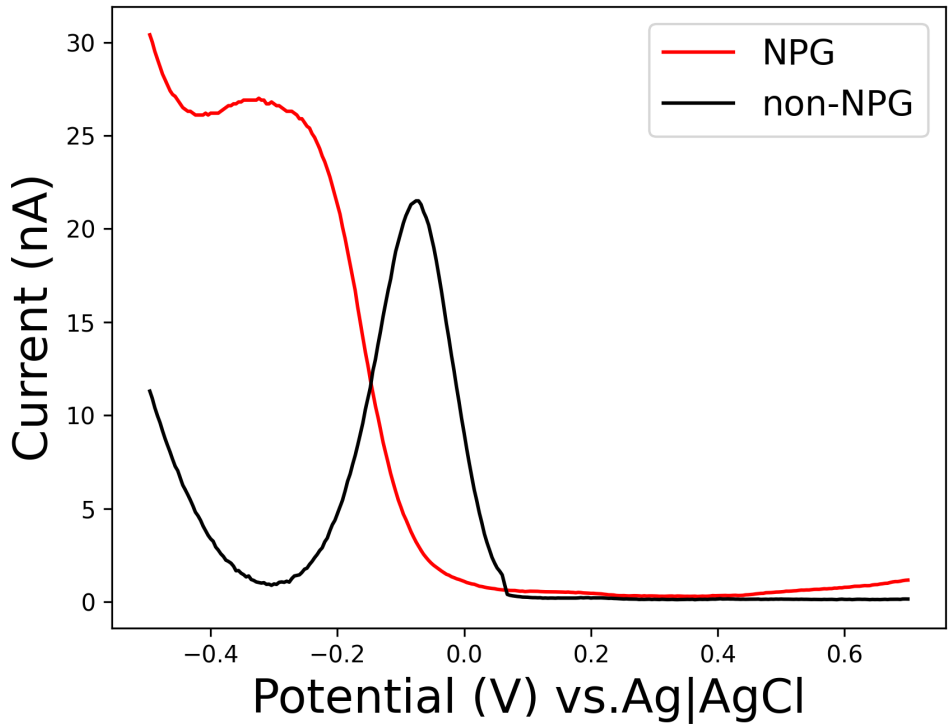

Figure 32: SWV of the non-NPG and NPG electrodes.

4.5.3 Surface area measurements

Because the CV recorded in ferrocenemethanol was unexpectedly similar before and after NPG formation, the electrode surfaces were cleaned in the same way that Jia et al. cleaned their electrodes [8] with the hope that minimizing methodological differences would yield more similar results. Voltammetric cycling was therefore conducted with the NPG electrode and one non-NPG electrode in 0.5 M H_2SO_4 with a Pt wire CE and $Cu|CuSO_4$ RE between 0.47 V and 1.57 V at a scan rate

of 0.1 V/s until the curves of subsequent cycles were no longer changing. The reduction peak of the first cycle was used to calculate the real areas, and voltammograms showing the first cycle for the electrodes can be found in the appendix. The non-NPG electrode was determined to have a real area of 729 μm^2, while the NPG electrode had a real area of 1556 μm^2. While it is impossible to say exactly how much the NPG formation increased the surface area by, since the area was not measured on the NPG electrode before the treatment, comparisons between these two electrodes can serve as an approximation, bearing in mind the variability in geometric area shown in table 1. The real area of the NPG electrode was more than twice the real area of the non-NPG electrode. Although such variability can be seen in the geometric areas in table 1, e.g. between electrodes 1 and 4, the fact that the NPG electrode had a geometric area of 225 μm^2, and that SEM images of the surfaces of NPG-treated and untreated electrodes show a clear difference in surface area, makes it likely that the much larger real area was caused by nanopore formation. The geometric area was estimated based on the SEM image in figure 26, and an SEM image found in the appendix, which shows the electrode from a different angle so that the whole gold surface could be taken into account. This means that the NPG electrode had a roughness factor of 6.92. This is not as large as the values reported by Jia et al. [8], but it is still much larger than would be expected of an unmodified surface.

5 Conclusion and future work

5.1 Conclusions

Disc-shaped gold microwire electrodes were fabricated and their electrochemical behavior was partially characterized. One NPG electrode was successfully produced by dealloying, but experimental conditions need to be optimized to achieve reproducibility. The superior sensitivity of the NPG electrode to hydrogen peroxide was shown with amperometry at 0.8 V, and its larger surface area was demonstrated with CV in $K_3Fe(CN)_6$, with SEM, and with electrochemical real surface area measurements in H_2SO_4. The anodization method did not successfully produce any NPG electrodes. Although epoxy, paraffin wax, phenol-allylphenol copolymer and Nafion™ have all been successfully used to insulate carbon electrodes, these materials do not effectively wet the surface of gold, so some other approach is needed to insulate gold microwire electrodes, either by finding a different insulator entirely, or a material that wets the gold surface and can then be coated with the aforementioned insulators.

5.2 Future work

The next step in making the NPG electrode viable for neuroscience research is to anchor the neccessary enzymes to its surface and using them to detect the release of acetylcholine and glutamate from neural spheroids. To do this efficently though, the nanopore formation step needs to be optimized and reasons for previous failure investigated. Further, their performance should be compared with electrodes modified with precious metal nanoparticles, as if these types of electrode would give similar responses a choice can be made based on which is easier and more reliable to fabricate. Another surface modification that may be of interest is adding polymer brushes, which could theoretically provide better attatchment for the enzymes compared with the bare gold surface. Finally, the one-step fabrication of gold nanotip electrodes *via* the micropipette puller method should be explored, since this method is much simpler than other methods that are currently popular.

References

[1] A. Oleinick, F. Lemaître, M. G. Collignon, I. Svir, and C. Amatore, "Vesicular release of neurotransmitters: Converting amperometric measurements into size, dynamics and energetics of initial fusion pores," *Faraday Discuss.*, vol. 164, pp. 33–55, 0 2013. DOI: 10.1039/C3FD00028A.

[2] S. D. Niyonambaza et al., "A review of neurotransmitters sensing methods for neuroengineering research," *Applied Sciences*, vol. 9, no. 21, 2019, ISSN: 2076-3417. DOI: 10.3390/app9214719.

[3] E. S. Bucher and R. M. Wightman, "Electrochemical analysis of neurotransmitters," *Annual Review of Analytical Chemistry*, vol. 8, pp. 239–261, 2015, ISSN: 1936-1335. DOI: 10.1146/annurev-anchem-071114-040426.

[4] B. Ostertag and A. Ross, "Editors' choice—review—the future of carbon-based neurochemical sensing: A critical perspective," *ECS Sensors Plus*, vol. 2, no. 4, 2023. DOI: 10.1149/2754-2726/ad15a2.

[5] L. Lu, Y. Dong, J. Wang, Q. Li, and X. Wu, "Direct electrochemistry and bioelectrocatalysis of horseradish peroxidase entrapped in a self-supporting nanoporous gold electrode: A new strategy to improve the orientation of immobilized enzymes," *Analytical Methods*, vol. 7, pp. 6686–6694, 16 2015. DOI: 10.1039/C5AY01333J.

[6] U. P. Do, F. Seland, and E. A. Johannessen, "The real area of nanoporous catalytic surfaces of gold and palladium in aqueous solutions," *Journal of The Electrochemical Society*, vol. 165, no. 5, H219, Mar. 2018. DOI: 10.1149/2.0341805jes.

[7] A. Sukeri, L. P. H. Saravia, and M. Bertotti, "A facile electrochemical approach to fabricate a nanoporous gold film electrode and its electrocatalytic activity towards dissolved oxygen reduction," *Physical Chemistry Chemical Physics*, vol. 17, pp. 28 510–28 514, 43 2015. DOI: 10.1039/C5CP05220C.

[8] F. Jia, C. Yu, Z. Ai, and L. Zhang, "Fabrication of Nanoporous Gold Film Electrodes with Ultrahigh Surface Area and Electrochemical Activity," *Chemistry of Materials*, vol. 19, no. 15, pp. 3648–3653, 2007. DOI: 10.1021/cm0704251.

[9] A. M. Downs et al., "Nanoporous gold for the miniaturization of in vivo electrochemical aptamer-based sensors," *ACS Sensors*, vol. 6, no. 6, pp. 2299–2306, 2021, PMID: 34038076. DOI: 10.1021/acssensors.1c00354.

[10] A. S. Nugraha, N. Amiralian, M. S. A. Hossain, and Y. Yamauchi, "Nanoporous gold architectures: Design, function, and emerging applications," *npj Materials Sustainability*, vol. 3, no. 37, 2025, ISSN: 2948-1775. DOI: 10.1038/s44296-025-00077-5.

[11] G. Wittstock et al., "Nanoporous gold: From structure evolution to functional properties in catalysis and electrochemistry," *Chemical Reviews*, vol. 123, no. 10, pp. 6716–6792, 2023, PMID: 37133401. DOI: 10.1021/acs.chemrev.2c00751.

[12] M. K. Masud et al., "Nanostructured mesoporous gold biosensor for microrna detection at attomolar level," *Biosensors and Bioelectronics*, vol. 168, p. 112 429, 2020, ISSN: 0956-5663. DOI: 10.1016/j.bios.2020.112429.

[13] S. H. Kim, "Nanoporous gold: Preparation and applications to catalysis and sensors," *Current Applied Physics*, vol. 18, no. 7, pp. 810–818, 2018, ISSN: 1567-1739. DOI: 10.1016/j.cap.2018.03.021.

[14] A. R. Heiskanen, C. F. Spégel, N. Kostesha, T. Ruzgas, and J. Emnéus, "Monitoring of Saccharomyces cerevisiae Cell Proliferation on Thiol-Modified Planar Gold Microelectrodes Using Impedance Spectroscopy," *Langmuir*, vol. 24, no. 16, pp. 9066–9073, 2008, PMID: 18630975. DOI: 10.1021/la800580f.

[15] L. M. Fischer et al., "Gold cleaning methods for electrochemical detection applications," *Microelectronic Engineering*, vol. 86, no. 4, pp. 1282–1285, 2009, MNE '08, ISSN: 0167-9317. DOI: 10.1016/j.mee.2008.11.045.

[16] D. Rand and R. Woods, "The nature of adsorbed oxygen on rhodium, palladium and gold electrodes," *Journal of Electroanalytical Chemistry and Interfacial Electrochemistry*, vol. 31, no. 1, pp. 29–38, 1971, ISSN: 0022-0728. DOI: 10.1016/S0022-0728(71)80039-6.

[17] B. Piela and P. K. Wrona, "Capacitance of the gold electrode in 0.5 M H2SO4 solution: a.c. impedance studies," *Journal of Electroanalytical Chemistry*, vol. 388, no. 1, pp. 69–79, 1995, ISSN: 1572-6657. DOI: 10.1016/0022-0728(94)03848-W.

[18] A. J. Bard and L. R. Faulkner, "Electrochemical methods: Fundamentals and applications," in 2nd ed. New York, NY: John Wiley Sons, Inc., 2001, pp. 171–174, ISBN: 978-1-118-31280-3.

[19] T. G. Strein and A. G. Ewing, "Characterization of submicron-sized carbon electrodes insulated with a phenol-allylphenol copolymer," *Analytical Chemistry*, vol. 64, no. 13, pp. 1368–1373, 1992. DOI: 10.1021/ac00037a012.

[20] J. Velmurugan, P. Sun, and M. V. Mirkin, "Scanning electrochemical microscopy with gold nanotips: The effect of electrode material on electron transfer rates," *The Journal of Physical Chemistry C*, vol. 113, no. 1, pp. 459–464, 2009. DOI: 10.1021/jp808632w.

[21] P. Sun and M. V. Mirkin, "Kinetics of electron-transfer reactions at nanoelectrodes," *Analytical Chemistry*, vol. 78, no. 18, pp. 6526–6534, 2006, PMID: 16970330. DOI: 10.1021/ac060924q.

[22] Y. Shao, M. V. Mirkin, G. Fish, S. Kokotov, D. Palanker, and A. Lewis, "Nanometer-sized electrochemical sensors," *Analytical Chemistry*, vol. 69, no. 8, pp. 1627–1634, 1997. DOI: 10.1021/ac960887a.

[23] G. Fish et al., "Ultrafast response micropipette-based submicrometer thermocouple," *Review of Scientific Instruments*, vol. 66, no. 5, pp. 3300–3306, May 1995, ISSN: 0034-6748. DOI: 10.1063/1.1145498.

[24] J. F. Cassidy, R. C. de Carvalho, and A. J. Betts, "Use of inner/outer sphere terminology in electrochemistry—a hexacyanoferrate ii/iii case study," *Electrochem*, vol. 4, no. 3, pp. 313–349, 2023, ISSN: 2673-3293. DOI: 10.3390/electrochem4030022.

[25] P. Gupta et al., "Temperature and time-controlled etching of carbon fiber nanotip electrodes: Creating nanocavity- and nanodot-modified surfaces for enhanced neurotransmitter detection," *Carbon*, vol. 243, p. 120 612, 2025, ISSN: 0008-6223. DOI: 10.1016/j.carbon.2025.120612.

[26] W. T. E. van den Beld et al., "In-situ raman spectroscopy to elucidate the influence of adsorption in graphene electrochemistry," *Scientific Reports*, vol. 7, no. 45080, 2017, ISSN: 2045-2322. DOI: 10.1038/srep45080.

6 Appendix

6.1 Voltammograms for real surface area determination

The first cycles of the CVs recorded in H_2SO_4 for the NPG and non-NPG electrodes are shown in figure 33. The cathodic peaks were used to acquire the real areas of these electrodes.

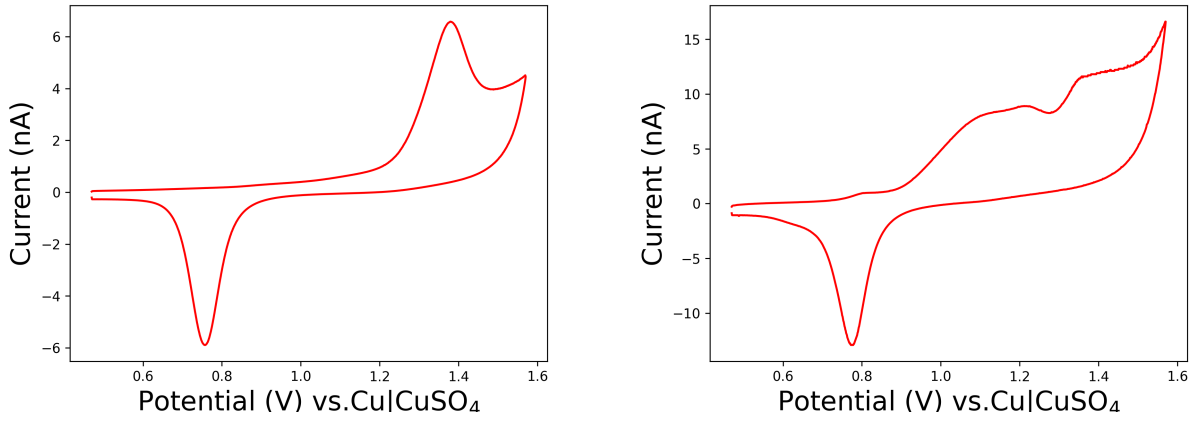

(a) (b)

Figure 33: CVs recorded in 0.5 M H_2SO_4 at 0.1 V/s

6.2 EDX images of failed NPG electrodes

Images from the EDX analysis of the failed NPG-electrodes in figure 27 are shown in figures 34 and 35.

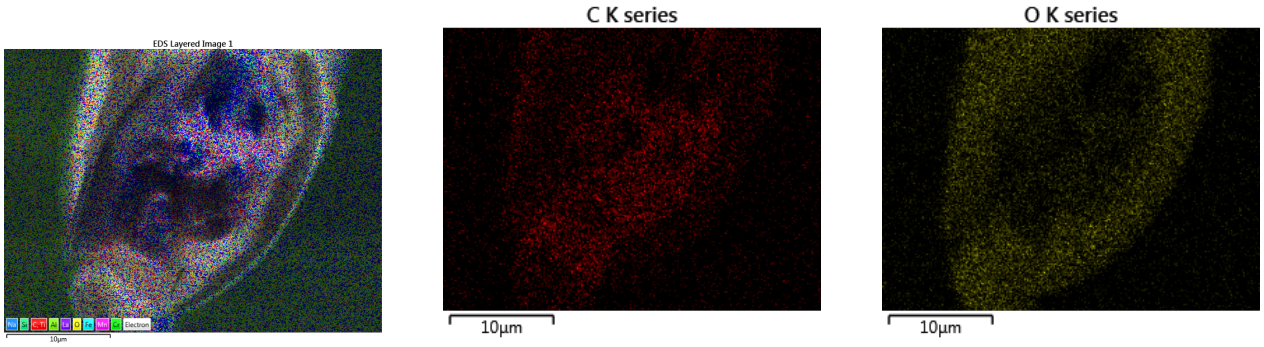

(a) (b) (c)

Figure 34: EDX images of the failed NPG electrode in figure 27a. Scale bars = 10 µm

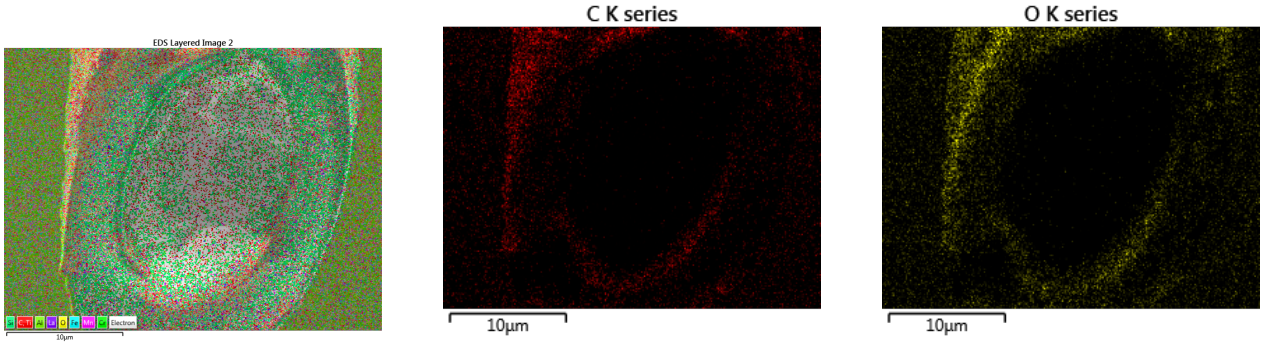

(a) (b) (c)

Figure 35: EDX images of the failed NPG electrode in figure 27b. Scale bars = 10 µm

6.3 SEM images of the NPG electrode for determination of A_{geo}

An SEM image of the NPG electrode taken from a different angle is shown in figure 36. This was used together with the SEM image in figure 26 to estimate the geometric area of the electrode.

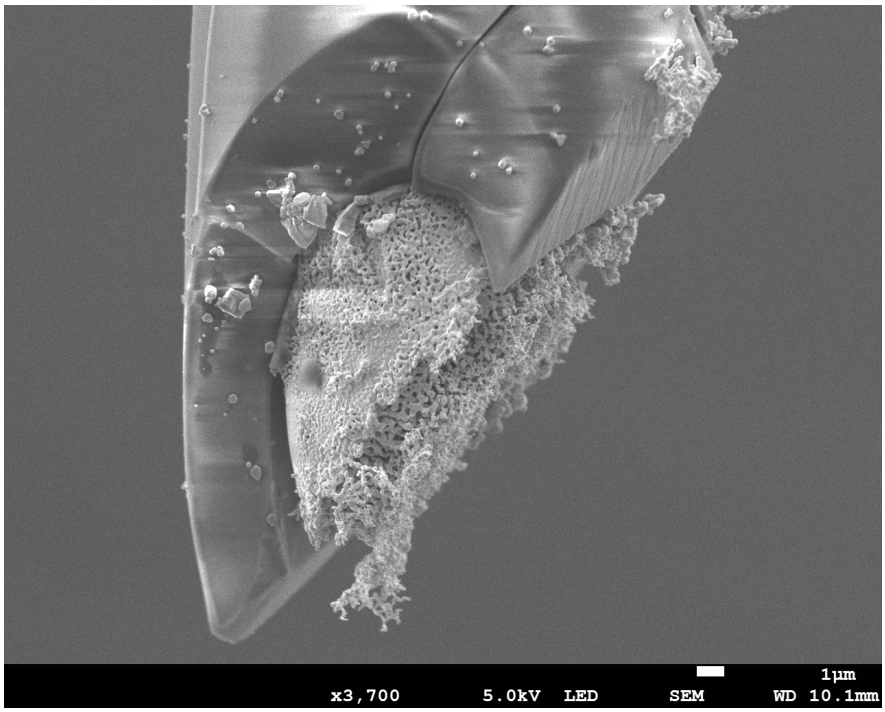

Figure 36: SEM image of the successful NPG electrode from a different angle. Scale bar = 1 µm.



CHALMERS
UNIVERSITY OF TECHNOLOGY